Title: The role of higher order thalamus during learning and correct performance in goal-directed behavior

Authors: D. LaTerra[1], M. Rosier[1], A.S. Bjerre[1], R. Masuda[1], T. Ryan[2] and L.M. Palmer[1*]

Affiliations:

[1]Florey Institute of Neuroscience and Mental Health, University of Melbourne, Victoria, 3010, Australia

[2]School of Biochemistry and Immunology and Trinity College Institute for Neuroscience, Trinity College Dublin, Dublin, D02 PN40, Ireland

Corresponding Author: Lucy M. Palmer; Florey Institute of Neuroscience and Mental Health, University of Melbourne, Victoria, Australia 3010**;** Ph: +61 3 9035 6022**;** Email: lucy.palmer@florey.edu.au

ABSTRACT

The thalamus is a gateway to the cortex. Cortical encoding of complex behavior can therefore only be understood by considering the thalamic processing of sensory and internally-generated information. Here, we use two-photon Ca^{2+} imaging and optogenetics to investigate the role of axonal projections from the posteromedial nucleus of the thalamus (POm) to the forepaw area of the mouse primary somatosensory cortex (forepaw S1). By recording the activity of POm axonal projections within forepaw S1 during expert and chance performance in two tactile goal-directed tasks, we demonstrate that POm axons increase activity in the response and, to a lesser extent, reward epochs specifically during correct HIT performance. When performing at chance level during learning of a new behavior, POm axonal activity was decreased to naïve rates and did not correlate with task performance. However, once evoked, the Ca^{2+} transients were larger than during expert performance, suggesting POm input to S1 differentially encodes chance and expert performance. Furthermore, the POm influences goal-directed behavior, as photo-inactivation of archaerhodopsin-expressing neurons in the POm decreased the learning rate and overall success in the behavioral task. Taken together, these findings expand the known roles of the higher-thalamic nuclei, illustrating the POm encodes and influences correct action during learning and performance in a sensory-based goal-directed behavior.

INTRODUCTION

Goal-directed behavior is crucial for survival in a dynamic environment. It involves the encoding and integration of sensory information that leads to specific rewarded behaviors (Kepecs et al., 2008; Li et al., 2015; Takahashi et al., 2016; Xu et al., 2012). This process must be dynamic, as flexible switching of learnt behaviors is required throughout life. The thalamus is a fundamental hub for the transfer of sensory information to the cortex, sending and receiving widespread innervation from numerous cortical and subcortical structures (Oh et al., 2014; Sherman and Guillery, 1996). Despite being positioned to coordinate the relay and integration of sensory information required during sensory-based behavior, historically, the thalamus has been viewed as a passive sensory relay center with negligible contribution to higher-order brain function and behavior. Recent studies have challenged this classical view, illustrating the thalamus plays crucial roles in cognitive tasks such as attention (Schmitt et al., 2017; Wimmer et al., 2015; Zhou et al., 2016), sensory perception (Saalmann and Kastner, 2011; Wilke et al., 2009), motor preparation and suppression (Casagrande et al., 2005; Yu et al., 2016), cortical plasticity (Audette et al., 2019; Gambino et al., 2014) and learning (Williams and Holtmaat, 2019).

The higher order thalamus is an enigmatic class of non-specific (diffuse projecting) thalamic nuclei which send feedback input to sensory cortical areas (Sherman and Guillery, 1996). These thalamic nuclei are thought to play an important role in behavioral flexibility (Wimmer *et al.*, 2015) as reported changes in firing patterns within the higher order thalamus (Ramcharan et al., 2005; Urbain et al., 2015) may underlie cortical state changes during adaptive behavior (Bruno and Sakmann, 2006; Poulet et al., 2012). Specifically, the postero-medial nucleus of the thalamus (POm) is the higher order thalamic nucleus subtending sensory processing in the primary somatosensory cortex (S1) (Deschenes et al., 1998; Jones, 2007). Sending dense projections to

layer 1 and layer 5 of S1(Meyer et al., 2010), the POm specifically targets a complex cortical microcircuit (Audette et al., 2017) which influences the encoding of somatosensory inputs (Castejon et al., 2016; Mease et al., 2016; Urbain *et al.*, 2015; Zhang and Bruno, 2019) and decision-related information (El-Boustani et al., 2020). POm is reciprocally connected with S1, but also receives and sends projections to secondary sensory, motor, premotor, and association cortices as well as many subcortical regions including the zona incerta and striatum (Alloway et al., 2017; Oh *et al.*, 2014; Trageser and Keller, 2004; Yamawaki and Shepherd, 2015). Based on its influence on cortical sensory processing and known extensive connectivity, the POm may play an important role during learning and performance in behaviors which require both the perception and integration of sensory information, such as sensory-based goal-directed behavior. To test this, we used two-photon Ca^{2+} imaging and optogenetics to investigate the role of POm projections in the forepaw S1 during learning, and chance and expert performance in tactile goal-directed behavior.

RESULTS

Ca^{2+} imaging of POm axonal projections in forepaw S1 during 'action' goal-directed behavior

To assess the activity of POm projection axons during tactile-based behavior, two-photon Ca^{2+} imaging of POm axons projecting to forepaw S1 was performed in mice (p50 - 70) previously injected with the Ca^{2+} indicator GCaMP6f (AAV1.Syn.GCaMP6f.WPRE.SV40) into the POm (see Methods; Figure 1A - figure supplement 1). Mice were then trained to associate forepaw tactile stimulation (200 Hz, 500 ms) with a reward in a goal-directed tactile detection task (see Methods; Figure 1B). If mice correctly responded by licking a reward port within 1.5 sec after receiving the

tactile stimulus, a sucrose water reward (10 % sucrose water) was delivered. We refer to this behavioral paradigm as 'action' goal-directed task (action task). Mice rapidly learnt this task, taking on average 4.38 ± 0.37 days to reach expert level (> 80 % correct responses to tactile stimulation; Figure 1 - figure supplement 2). Once expert, Ca^{2+} transients were recorded from POm axons that project to layer 1 of the forepaw S1 (48 ± 6.8 µm from the pia surface; Figures 1C, D and Figure 1 - figure supplement 3). POm axons were excluded if they had greater than 95 % correlated activity with other axons within the POm (see methods and Figure 1 - figure supplement 4). During correct performance in the tactile goal-directed task, large Ca^{2+} transients (>2 s.d of the baseline fluorescence; see Methods) were evoked in 90 % of POm axons. This task-evoked POm axonal activity was greater than tactile-evoked Ca^{2+} activity in the naïve state, with a significantly higher probability of evoking a Ca^{2+} transient in POm axons during the tactile task (0.35 ± 0.03 vs 0.21 ± 0.02; $p = 0.0007$; Figures 1 E and Figure 1 – figure supplement 5). Once evoked, the amplitude of the Ca^{2+} transients were not significantly different between naïve and expert mice ($p = 0.58$; F test). To further assess the activity of POm axons during tactile goal-directed behavior, we categorized all axons according to their peak activity during baseline (-2 to -1 s pre-stimulus), stimulus/response (response; 0 to 1 s post-stimulus) or reward (2 to 3 s post-stimulus) epochs of the task (Figure 1F). Since, during expert behavior, only a small portion of axons responded during the stimulus epoch alone (6 %; see Methods), the stimulus and response epoch were merged. Here, POm axonal activity was greatest during the response epoch, increasing signaling by more than 4-fold above baseline (probability per trial, 0.32 ± 0.02 vs 0.08 ± 0.003; n = 418 axons, 11 mice; $p < 0.0001$; Figure 1G). POm axons also significantly increased activity above baseline during the reward epoch (probability per trial, 0.12 ± 0.007; n = 418 axons, 11 mice, $p < 0.0225$). However, when compared with the response-evoked activity, active POm axons were reduced in number (n

= 275 vs 359 axons) and evoked rate (probability per trial, $p < 0.0001$), suggesting that POm axons preferentially encode the response epoch (Figure 1G). Direct comparison of the Ca^{2+} transient amplitudes from POm axons with both spontaneous and evoked activity (n = 239 axons, 11 mice) illustrates that Ca^{2+} transients evoked during the response epoch (0.97 ± 0.04 $\Delta F/F$) were also significantly larger than transients evoked during both baseline (0.756 ± 0.02 $\Delta F/F$, $p = 0.0005$) and reward delivery (0.679 ± 0.0219 $\Delta F/F$; $p < 0.0001$), further highlighting the enhanced POm axonal signaling during the behavioral response (Figure 1H). Together, these results illustrate that the POm increases signaling in S1 during both response and reward delivery, with greatest activity during the behavioral response to tactile goal-directed behavior. Licking motion itself did not influence POm axon activity in forepaw S1, as there was no correlation between licking frequency and POm axonal activity ($p = 0.923$; Figure 1I). Furthermore, there was no detectable change from baseline in POm axonal Ca^{2+} activity during spontaneous licking (0.09 ± 0.027 Hz; $p = 0.29$; n = 71 axons, 3 mice). Therefore, overall, POm axons in forepaw S1 encode response and, to a lesser extent, reward information during a tactile goal-directed task.

POm axon activity in forepaw S1 is correlated with correct tactile goal-directed behavior

We next assessed whether POm axonal activity in forepaw S1 changes according to behavioral performance. Upon receiving a tactile stimulus in the action task, mice had to lick a reward port within 1.5s to receive a sucrose water reward (HIT). However, if they did not respond during this epoch, then no water was delivered (MISS; Figure 2A). Despite performing at expert level, mice did not respond (MISS) to on average 12.63 ± 6.63 % of tactile stimuli. To assess whether the activity of POm axons is also correlated with MISS behavior, evoked Ca^{2+} activity was directly compared in POm axons with both HIT and MISS activity (n = 159 axons, 6 mice). Compared to

correct HIT behavior, POm axons in forepaw S1 were overall less active during MISS trials (Figure 2B). In addition to an overall decrease in the number of axons active throughout the entire tactile goal-directed task (by 51%), there was also a significant decrease in the probability of evoking an axonal Ca^{2+} event during the behavioral response in MISS trials (paired; HIT, 0.27 ± 0.02; MISS, 0.12 ± 0.01; $p < 0.0001$; Figure 2C). In contrast, the peak amplitude of the evoked Ca^{2+} transients were similar during HIT and MISS trials (paired; response; HIT, 0.954 ± 0.08; MISS 0.888 ± 0.08; $p = 0.470$ n = 82 axons; reward; HIT, 0.635 ± 0.04; MISS, 0.708 ± 0.06; $p = 0.252$; n = 73 axons, 6 mice). Behaviorally speaking, HIT and MISS trials differ in the mouse movement, which has been shown to increase overall brain activity (Stringer et al., 2019). To investigate whether the increased POm axonal activity during the HIT response to tactile goal-directed behavior is due to body movement, we compared the evoked Ca^{2+} activity in POm axons with catch trials where mice spontaneously licked for reward (false alarm). Despite licking during false alarm trials, POm axons were significantly less active than during HIT trials (unpaired, probability per trial, 0.15 ± 0.01, n = 239 axons, 10 mice, $p < 0.0001$; Figure 2C). Since there was no significant difference between FA and HIT licking rates ($p = 0.203$; n = 9 mice), this data further suggests that POm axonal activity is not simply due to licking behavior. There was also a significant decrease in the probability of evoking an axonal Ca^{2+} event during the reward epoch in MISS trials (HIT, 0.13 ± 0.02; MISS, 0.09 ± 0.01; $p = 0.0408$; n = 159 axons, 6 mice; Figure 2D). During MISS trials, POm axonal activity was similar to baseline rates (0.07 ± 0.007; $p > 0.999$; n = 159 axons, 6 mice; Figure 2D). Together, this data suggests that the POm encodes behavioral performance, increasing signaling between the POm and forepaw S1 during correct HIT behavior during both the response and reward epochs in a tactile goal-directed task.

POm axon activity in forepaw S1 during suppression of a goal-directed action

Goal-directed behavior requires motor actions to be suppressed once they are no longer appropriate to achieve the current goal (Jahanshahi et al., 2015). To investigate the involvement of the higher order thalamus during suppression of a previously learned goal-directed action, we performed Ca^{2+} imaging from POm axons during a modified goal-directed paradigm. Here, mice previously injected with the Ca^{2+} indicator GCaMP6f in the POm were trained in the 'action' goal-directed task (as above). Once expert (> 80 % correct responses to tactile stimulation), the behavioral paradigm was changed such that the mice only received the reward if they suppressed licking in response to the tactile stimulus (Figure 3A). We refer to this behavioral paradigm as 'action-suppression' goal-directed task (suppression task). To monitor cognitive arousal (Bradley et al., 2008), dynamic changes in pupil diameter were recorded while mice were performing the behavioral tasks. Despite the enforced behavioral (licking) suppression, the pupil diameter was significantly increased from baseline during the behavior (0.32 ± 0.05 to 0.44 ± 0.07; $p = 0.031$; n = 6 mice), indicating mice were engaged in the task. When compared with the action goal-directed task, there was no significant difference in peak pupil diameter during the pre-trial baseline (0.32 ± 0.05 vs 0.29 ± 0.06 mm, $p = 0.312$), pre-tactile (0.35 ± 0.06 vs 0.31 ± 0.07 mm, $p = 0.219$), and post-tactile (0.44 ± 0.07 vs 0.41 ± 0.09 mm; $p = 0.687$; n = 6 mice; Figure 3B). Furthermore, there was no significant difference in correct performance rates during the action (83 ± 5 % correct; n = 11 mice) and suppression (86 ± 7 %; n = 6 mice; $p = 0.57$) tasks. POm projections in S1 were highly active during the suppression task, with evoked Ca^{2+} transients that were significantly larger in amplitude than spontaneous activity (0.99 ± 0.06 $\Delta F/F$ vs 1.19 ± 0.06 $\Delta F/F$; n = 144 axons, 6 mice; $p = 0.0002$). Similar to the action task, POm axons were most active during the response epoch in correct HIT trials (evoked rate, 0.24 ± 0.03; n = 144 axons, 6 mice; Figure 3C). Therefore,

since the suppression task requires mice to suppress licking during the response epoch, the increased response activity was not correlated with licking behavior. To assess whether POm activity reflected behavioral performance in the suppression task, evoked POm Ca^{2+} activity was directly compared during MISS trials. Similar to the action task, POm axons in forepaw S1 were less active during MISS behavior, with a significant decrease in the probability of response-evoked activity in MISS trials compared to HIT trials (HIT, 0.24 ± 0.03 vs MISS, 0.15 ± 0.03; n = 144/53 axons, 6 mice; p = 0.029; Figure 3D). Here, MISS behavior involves incorrectly licking for reward during the response epoch, further suggesting that POm axonal activity in S1 does not signal licking behavior. Taken together, in both the action and suppression tasks, POm axons in forepaw S1 preferentially encode the response epoch during correct performance (HIT trials). On average, the peak amplitudes (1.19 ± 0.06 vs 1.26 ± 0.05 $\Delta F/F$, p = 0.3812) and durations (623 ± 50 vs 666 ± 35 ms; p = 0.2234) of Ca^{2+} transients evoked during the action and suppression tasks were comparable (Figure 3F). However, during the suppression task, the probability of POm signaling during the response epoch was significantly decreased compared to the action task (p = 0.0007; Figure 3F). This contrasts with the similar probability of evoked POm signaling during the reward epoch (p = 0.87; Figure 3F). Together, these results further support the increased signaling of POm axons within forepaw S1 during correct (HIT) goal-directed active behavior.

POm axon activity during switching of tactile goal-directed behavior

Flexibly switching motor actions in response to changing conditions is crucial for survival. Termed 'behavioral flexibility', this enables changes in the behavioral response to sensory information in dynamic environments. To investigate the role of POm during switching of rewarded behavior, we performed Ca^{2+} imaging from POm axons in forepaw S1 as mice transitioned from the 'action'

goal-directed task to the 'action-suppression' goal-directed task (Figure 4A). We refer to this behavioral paradigm as 'switching'. On average mouse performance returned to chance level (50 % correct performance) 2.25 ± 0.47 training sessions after switching the rewarded behavior. To monitor task engagement, pupil tracking was performed during the switch in behavior. Compared with correct performance in the active goal-directed behavior, there was no significant difference in pupil peak diameter during pre-trial baseline (0.28 ± 0.05 vs 0.30 ± 0.07mm, p = 0.6871, n = 6 mice), pre-tactile (0.29 ± 0.05 vs 0.32 ± 0.07, p = 0.4372, n = 6 mice) and post-tactile epochs (0.40 ± 0.06 vs 0.43 ± 0.01; p = 0.6874; n = 6 mice, Figure 4B). Although equally engaged in the task, the activity of POm axonal projections in forepaw S1 was overall reduced during chance (50 % correct) non-expert behavior. Unlike expert behavior, the evoked rate of POm activity during chance performance did not reflect task performance, with similar evoked rates during both HIT (no lick, rewarded) and MISS (lick, unrewarded) responses (probability per trial, 0.15 ± 0.02 vs 0.15 ± 0.01, p = 0.74; n = 121 axons, 4 mice; Figure 4C - E). This rate of evoked activity during chance performance was similar to naïve mice (p = 0.159), and significantly reduced when compared to expert performance (Figure 4E). Furthermore, during chance performance in non-expert mice, POm projections in S1 did not signal correct performance nor reward delivery as there was no difference in the evoked rate of POm axonal Ca^{2+} activity during the behavioral response and reward epochs (probability per trial, 0.15 ± 0.02 vs 0.14 ± 0.02; p = 0.62; n = 121 axons, 4 mice). Taken together, unlike expert behavior, POm axonal activity in forepaw S1 was reduced and not correlated with the behavioral response during chance, non-expert, performance in a goal-directed task.

To further investigate the potential role of the POm in behavioral switching, direct comparison of the amplitude of POm axonal transients was performed in mice which performed all tasks (Action,

Switch and Suppression task; n = 4 mice). Although POm axons were less active overall, when evoked, the amplitude of Ca^{2+} transients evoked during HIT (Action, 1.19 ± 0.08 ΔF/F; Switch, 1.51 ± 0.09 ΔF/F, Suppression, 1.13 ± 0.09 ΔF/F; p = 0.0003; n = 77/69/47 axons, 4 mice; Figure 4F) and MISS (Action, 0.76 ± 0.05 ΔF/F; Switch, 1.37 ± 0.07 ΔF/F, Suppression, 1.02 ± 0.08 ΔF/F; p = 0.0001; n = 79/88/30 axons, 4 mice) performance during chance behavior were significantly larger than expert behavior. The lower evoked rate, but larger POm axonal transients during chance performance in a goal-directed task suggests a shift in the activity of POm input to forepaw S1 during non-expert behavior, as mice are adjusting their behavioral strategy while learning the new goal-directed task.

The influence of POm input during expert goal-directed behavior

The results above suggest the POm axonal activity in forepaw S1 is greatest during correct HIT behavioral response during expert, but not chance, performance in tactile goal-directed behavior. To investigate the role of this POm input on the correct performance during expert behavior, the POm was photo-inhibited while expert mice performed the goal-directed task. Here, the inhibitory opsin, archaerhodopsin (ArchT; AAV1.CAG.ArchT.GFP.WPRE.SV40, 60 nl) was unilaterally injected into the POm. First, the effectiveness of 565 nm LED photo-inhibition of POm neurons expressing ArchT was tested using patch clamp electrophysiology in the thalamic brain-slice preparation. Although photo-inhibition did not completely abolish action potentials in POm neurons, the evoked firing rate was significantly decreased by 64 ± 13 % (p = 0.031; n = 6 neurons; Figure 5 – figure supplement 1). Next, we tested the influence of this decrease in POm activity on active goal-directed behavior in expert mice. A fiber-optic cannula was chronically inserted into the POm which was previously injected with ArchT (see methods and Figure 5A) and mice were

trained in the 'action' goal-directed task. Importantly, the duration of training and baseline performance was not affected by the injection of the inhibitory opsin into the POm (Figure 5 – figure supplement 2). Once expert (> 80 % correct performance), the POm was initially photo-inactivated with interleaved yellow LED light (565 nm, 5 mW, 2 s) during the stim/response epoch as this was when the POm was most active during the behavior (see Methods). Our findings illustrate that partial photo-inactivation of the POm during the stimulus and response epoch produced a significant reduction in the overall behavioral performance (d prime, 2.58 ± 0.15 vs. 2.23 ± 0.26; n = 9 mice; p = 0.04; Figure 5B) while no change was observed in the control group injected with GFP in the POm (d prime, 2.62 ± 0.24 vs. 2.83 ± 0.29; n = 9 mice; p = 0.26; Figure 5 – figure supplement 2). Specifically, the reduction in correct performance following POm partial photo-inactivation was due to a significant decrease in performance during HIT trials (z-score, 2.09 ± 0.09 vs. 1.77 ± 0.15; n = 9 mice, p = 0.02) and not the rate of false alarms (z-score, -0.48 ± 0.16 vs. -0.46 ± 0.20; n = 9 mice, p = 0.82; Figure 5C). Despite this change in performance, POm photo-inactivation during the stim/response epoch did not alter licking behavior as there was no significant difference in the latency to the first lick (control, 351 ± 29 ms vs ArchT, 342 ± 26 ms, n = 9 mice, p = 0.1282, Figure 5D). The specific influence of POm partial photo-inactivation during the stim/response epoch is consistent with the increased signaling of POm axons within forepaw S1 during this epoch in expert mice (Figures 2 and 3). Since POm axons within S1 also increased activity above baseline during reward delivery, albeit less than during the behavioral response, we next tested whether photo-inactivation of the POm during the reward epoch influenced behavioral performance. Here, no change was observed in overall behavioral performance when POm was photo-inactivated during reward delivery (ArchT d prime, LED ON 3.54 ± 0.27 vs. LED OFF 3.64 ± 0.09; n = 5 mice; p = 0.99; Figure 5E). There was also no change

in overall behavioral performance during LED ON in reward delivery in control (GFP) mice (GFP d prime, LED ON 3.70 ± 0.19 vs. LED OFF 3.69 ± 0.12; n = 6 mice; p = 0.75). Furthermore, similar to photo-inactivation during the stim/response epoch, there was no influence on licking behavior when the POm was photo-inactivated during the reward epoch (Figure 5F). Taken together, decreasing POm activity during the stim/response epoch in expert mice influenced correct performance in a goal-directed task, suggesting the higher-order thalamus specifically influences correct, but not incorrect, goal-directed responses.

The influence of POm input during learning of goal-directed behavior

Our findings suggest that the POm changes activity patterns from naïve to expert performance, suggesting that the POm may play a role in learning of a sensory-based goal-directed task. To test this, a fiber-optic cannula was chronically inserted into the POm which was previously injected with ArchT and mice were trained in the 'action' goal-directed task. During each training session, the POm was photo-inactivated with yellow LED light (565 nm, 5 mW, 2 s) during the stim/response epoch as to not interfere with possible feedback pathways activated during reward, and this was also when the POm was most active during expert behavior. Here, when the POm was photo-inactivated during learning, mice took on average 7.6 ± 1.3 sessions to reach expert (> 80 % correct) performance (n = 5 mice; Figure 6A). This is significantly greater than the number of sessions it took to reach expert performance in mice that were either previously injected with ArchT with LED OFF during learning (3.6 ± 0.4; n = 9 mice) or GFP (LED ON during learning; 4.5 ± 0.2; n = 6 mice; p = 0.004; Figure 6B). Therefore, decreasing POm activity during training in the goal-directed task influenced the rate of learning, with mice requiring more sessions to reach

293 expert performance during POm photo-inactivation (Figure 6C). Together, these findings suggest
294 that the higher-order thalamus plays an important role in the learning of sensory-based tasks.
295 In summary, our findings suggest that POm axonal projections in forepaw S1 preferentially encode
296 the behavioral response during learning and correct performance in tactile goal-directed behavior.
297 Overall, POm axons were more active during expert performance, with greatest evoked rates in
298 active behavior which required licking for reward and POm photo-inactivation during learning of
299 the goal-directed behavior increased the number of training sessions required to reach expert
300 performance. Taken together, these findings suggest that POm input to forepaw S1 shifts in
301 strength and rate dynamically during learning and performance of a behavioral task, specifically
302 encoding correct goal-directed action in the expert mouse.
303
304 **DISCUSSION**
305 The results presented here highlight the role of the POm during sensory-based goal-directed
306 behavior. We used two-photon Ca^{2+} imaging to illustrate that POm axonal activity in forepaw S1
307 encodes correct behavioral response during expert performance in tactile goal-directed behavior.
308 Specifically, POm axons increased activity in the response and, to a lesser extent, reward epochs
309 during correct performance in expert behavior. This is in contrast to chance performance, where
310 POm axonal activity did not correlate with task performance. Furthermore, the POm influences
311 learning and performance in goal-directed behavior, as photo-inactivation of archaerhodopsin-
312 expressing neurons in the POm decreased learning rates and correct performance in expert
313 behavior. Taken together, these findings illustrate that POM input to S1 specifically encodes
314 correct performance during goal-directed behavior and influences sensory-based learning.

The POm is a higher order non-specific thalamic nucleus that is reciprocally connected with S1, but also receives and sends projections to motor, premotor, association cortices and the brainstem (Groh et al., 2014) as well as many subcortical regions including the zona incerta and striatum (Alloway *et al.*, 2017; Oh *et al.*, 2014; Trageser and Keller, 2004; Yamawaki and Shepherd, 2015). Given the extensive and heterogeneous organization of its afferent inputs, it is difficult to determine the input source driving POm activity during complex goal directed behavior. However, since the POm receives input from the primary motor cortex (Yamawaki and Shepherd, 2015), it could be speculated that the increased axonal activity during the behavioral response has a motor origin. In fact, previous studies have shown that the thalamus is a circuit hub in motor preparation (Guo et al., 2017). While a general increase in POm activity has been reported during active states (Urbain *et al.*, 2015), encoding of whisking related movement in the POm is relatively poor (Moore et al., 2015). In agreement, our findings illustrate that POm input in forepaw S1 does not specifically encode movement, as 1) POm activity is enhanced during the response epoch in both the action (licking) and suppression (no licking) tasks, 2) there is not a strong correlation between POm activity and licking frequency, and 3) POm activity is minimal during spontaneous licking and false alarm trials.

Here, we illustrate that POm activity is correlated with task performance in expert mice with greater signaling in POm axonal projections within forepaw S1 during correct HIT behavior in both the action and suppression task. Similar results were recently found in the thalamocortical circuit subserving the anterior lateral motor cortex (Takahashi et al., 2021) illustrating this may be a universal role of the thalamus. Although the POm encodes sensory information in naïve mice, in the expert state, our findings suggest that this increased activity in POm axons during the response epoch is not primarily due to enhanced sensory encoding. Here, despite receiving exactly the same

tactile stimulus, POm signaling in forepaw S1 is increased during correct HIT trials compared with MISS trials in both the action and suppression task. This difference in POm activity was not due to differences in licking behavior nor arousal, as POm activity was similar during the action and suppression tasks (which involved licking and not licking for reward) and did not reflect levels of arousal measured using pupil tracking. The difference in POm activity during the HIT and MISS trials was also not due to stimulus delivery as all experiments were monitored online via a behavioral camera to examine the location of the forepaw on the stimulus during all trials, and trials where the paw was not clearly resting on the stimulating rod were excluded from analysis. However, we cannot rule out that non-detectable changes in postures/paw grip may occur which may alter the effectiveness of the stimulus.

Although, overall, POm axons in forepaw S1 were predominantly active in the response epoch during correct performance in a tactile goal-directed behavior, the activity patterns of individual axons were heterogenous which may be due to a heterogenous population of POm neurons projecting to S1 (Clasca et al., 2012). Our findings illustrate that a subset of axons were correlated with the sensory stimulus and reward epoch during expert behavior. It is also possible that single POm axons may have heterogenous encoding which, since our findings are based on overall average activity per POm axonal projection, would not be evident in our study. Delving into encoding at the level of a single thalamic axon is an exciting direction for future research. How does POm encoding of goal-directed behavior compare to the activity of other thalamic nuclei which also project to forepaw S1? Of particular interest is the ventral posterolateral nucleus of the thalamus (VPL) which, in contrast to POm, targets the middle cortical layers of forepaw S1. Viewed as a feedforward (sensory) pathway, perhaps the VPL axons would be more active during the stimulus delivery and, in contrast to POm axons, their activity would be similar between the

different behavioral tasks (action, suppression, switch). It is of great interest to compare and contrast these different pathways to gain a holistic view of the role of the thalamus during goal-directed behavior, which will be the focus of exciting future studies.

In agreement with the POm axonal activity within S1, behavioral performance in expert mice was disrupted when the POm was photo-inactivated during the stimulus and response epoch, but not during reward delivery. Together, these results suggest that the POm predominantly encodes the behavioral response. The behavioral effect was small which may be due to the following. Firstly, we illustrate that photo-inhibiting LED light (565 nm) caused a significant decrease in the evoked action potential rate in POm neurons expressing Archaerhodopsin *in vitro*. Taking into account the high firing rate of POm neurons *in vivo*, photoinhibition would not completely abolish POm activity *in vivo*. Therefore, during the goal-directed behavior, the POm is presumably still active, albeit at a reduced rate. Secondly, there was large behavioral variability which may reflect different rates of transfection and optical fiber placement. Thirdly, previous studies have illustrated that similar sensory-based goal-directed behaviors do not require primary cortical areas (Hong et al., 2018). Therefore, it is not expected that partially inhibiting an input stream to the forepaw S1 would have a large effect on the behavioral performance. Combined with the reported increase in POm axonal activity during correct performance in expert mice, the influence of POm photo-inactivation on task performance further supports the finding that POm encodes correct performance in goal-directed action. In this study, POm was also photo-inactivated during learning of the tactile goal-directed behavior. Here, dampening POm activity significantly decreased the rate of learning, causing a greater than two-fold increase in the number of training sessions required to reach expert performance. In our study, the influence of POm photo-inactivation on goal-directed behavior was measurably greater during learning than expert performance, suggesting that

384 the POm plays a vital role in learning. The role of the POm during learning requires more in-depth
385 investigation, and since the POm targets many cortical and subcortical regions (Alloway *et al.*,
386 2017; Oh *et al.*, 2014; Trageser and Keller, 2004; Yamawaki and Shepherd, 2015), future studies
387 with target-specific photo-inhibition are required to illustrate which POm projection pathway
388 specifically influences the learning and execution of goal-directed behavior.
389 In this study, considerable effort was made to ensure the specific targeting of POm. The POm was
390 stereotaxically targeted with small volumes and the resulting fluorescence at both the thalamic
391 injection site and the cortical layer targeted by the axonal projections was scrutinized after every
392 experiment (Gambino et al., 2014). We note that our stereotaxic injections were not flawless and
393 virus occasionally spread into ventral posterior nuclei, or along the injection pipette track and into
394 high-order visual thalamic nuclei, superficial to POm. If fluorescence was detected in non-targeted
395 areas, then the experiments were excluded from analysis. It is possible that there was weak
396 (undetectable) expression outside of the POm, however, these neighboring thalamic nuclei do not
397 predominantly target layer 1 of the forepaw area of S1 (Kamishina et al., 2009; Meyer *et al.*, 2010;
398 van Groen and Wyss, 1992) and therefore would not significantly contribute to our calcium
399 imaging findings. In the optogenetic photo-inhibition experiments, targeting of the fiber optic
400 canula to the POm was confirmed after every experiment and weak expression of ArchT outside
401 of the POm would therefore also have minimal impact on our findings.
402 To probe whether thalamocortical projections to S1 are dynamic and change activity patterns
403 according to changes in reward expectation and delivery, we recorded the activity of POm axonal
404 projections in S1 following a switch in the task contingency. In accordance with thalamic function
405 playing an important role in behavioral flexibility (Wimmer *et al.*, 2015), evoked axonal Ca^{2+}
406 activity was altered during the switch in rewarded behavior, suggesting a shift in action potential

firing in POm thalamocortical neurons. Changes in firing mode have been reported in sensory higher order thalamus of behaving rodents and primates (Ramcharan *et al.*, 2005; Urbain *et al.*, 2015) and may underlie cortical state changes during uncertain conditions and changes in reward expectation (Bruno and Sakmann, 2006; Poulet *et al.*, 2012). These changes in firing patterns could drive different microcircuits (Allen et al., 2017; Morgenstern et al., 2016; Tye and Uchida, 2018) as POm inputs to the cortex directly target both excitatory and inhibitory neurons (Audette *et al.*, 2017) however, more in-depth studies are required to directly investigate the influence of changing POm input on cortical microcircuits. Increased activity in the higher order thalamus has also been associated with the expected value and significance of rewarded sensory stimuli (Komura et al., 2001) and may reflect learned-dependent strengthening of specific POm thalamocortical synapses (Audette *et al.*, 2019). Our findings show that POm activity is enhanced during reward delivery in the tactile goal-directed task, although the absolute POm signaling is less than during the behavioral response.

Considering that patterns of cortical activity during behavior have been associated with task engagement, brain state, attention, motivation or reward (Kobak et al., 2016; Lacefield et al., 2019; Poort et al., 2015; Poulet and Petersen, 2008; Reimer et al., 2014), we monitored pupil dynamics during the goal-directed tasks. We report that while overall POm activity increased concomitantly with pupil diameter during the behavioral response, this trend was reversed during reward delivery. By sorting POm axons according to their peak activity during the tactile goal-directed task, we revealed a subgroup of POm axons highly responsive during the reward epoch. This finding highlights the heterogeneity of the higher order thalamus, with subsets of POm axonal projections specifically encoding either the stimulus, response or reward delivery. In line with this finding, a recent report further supports the functional heterogeneity of POm cortical input and suggests it

has modulatory role in various brain regions during decision making in a goal-directed task (El-Boustani *et al.*, 2020). However, overall, the results presented here illustrate that the POm predominantly transfers behaviorally relevant information to forepaw S1 during the response epoch of goal-directed behavior. Specifically, POm input to S1 is greatest in the response epoch during correct HIT performance in expert behavior. Although this increased activity during the behavioral response epoch may not be necessary for maintaining the tactile information, these findings suggest that the POm does not simply encode sensory information, but it also reports behavioral outcome in learnt behavior and changes in behavioral state. Since the POm projects to various cortical and sub-cortical regions (Oh *et al.*, 2014; Yamashita et al., 2018), the POm may also send task-relevant to other brain regions (El-Boustani *et al.*, 2020). Likewise, since S1 also receives input from various brain regions, it would be of interest to investigate whether other input pathways send complimentary information during goal-directed behavior.

In summary, we show that the higher order thalamus encodes correct performance during goal-directed behavior and influences the rate of learning. This finding expands the known roles of the higher-thalamic nuclei, from sensory encoding to influencing learning and correct performance in goal-directed behavior. Overall, the thalamus is not a simple relay system. It encodes and influences learning of goal-directed behaviors which are crucial for survival in a dynamic environment.

MATERIALS AND METHODS

All procedures were approved by the Florey Institute of Neuroscience and Mental Health Animal Care and Ethics Committee (17-091-FINMH) and followed the guidelines of the Australian Code of Practice for the Care and Use of Animals for Scientific Purposes.

Mice. Wild type C57BL/6 female mice (PN30 - PN80) were used in this study. Mice were housed in groups of six in a 12:12 natural light/dark cycle. All behavioral tests were performed during the light phase.

Virus injection. All surgical procedures were conducted under isoflurane anesthesia (~1-2% in O2). Body temperature was maintained at ~36 °C and the depth of anesthesia was monitored throughout the experiment. Mice (~PN30 - 40) were placed in a stereotaxic frame (Narishige) and eye ointment was applied to the eye to prevent dehydration. The skin was disinfected with ethanol 70% and betadine before lidocaine (1%, wt/vol) was topically applied to the wound edges for additional local anesthesia. An incision in the skin (10 mm) was made to expose the skull and a small craniotomy (~0.5 × 0.5 mm) was made over the left posteromedial (POm) complex of the thalamus using the following stereotaxic coordinates: rostrocaudal (RC), −1.7 mm; mediolateral (ML), −1.25 mm; dorsoventral (DV), −3.00 mm from bregma. AAV1.Syn.GCaMP6f.WPRE.SV40 (Addgene plasmid # 100837, 1 x 10^{13} vg/mL) or AAV1.CAG.ArchT.GFP.WPRE.SV40 (Addgene plasmid # 29777, 1 x 10^{13} vg/mL) was slowly injected from a glass pipette (60 nl, Wiretrol, Drummond) for at least 5 min using an oil hydraulic manipulator system (MMO-220A, Narishige). The skin was then sutured and Meloxicam (3mg / Kg) was injected intraperitoneally (i.p.) for additional post-operative analgesia and anti-inflammatory action. Mice were then returned to their home cage for recovery.

Chronic cranial window surgery. Mice previously injected with the Ca^{2+} indicator GCaMP6f were anaesthetized (isoflurane, ~1-2 % in O2, vol/vol) and body temperature was maintained at ~36 °C and the depth of anesthesia was monitored throughout the experiment. Eye ointment was applied to prevent dehydration and the top of the head was disinfected with ethanol 70 % and betadine and lidocaine (1 %, wt/vol) was topically applied for additional local anesthesia. The skin

covering the skull was removed, and a craniotomy was performed over the left forepaw area of the primary somatosensory cortex (centered at coordinates: RC, 0 mm; ML, -2.3 mm; from bregma). The dura was left intact and a circular coverslip (3 mm diameter) was placed over the open craniotomy and seal-attached to the skull with acrylic glue. A custom-made aluminum head bar (2 x 1 x 0.1 cm) was then attached to the skull for head-fixation using dental cement (C&B metabond, Parkell Inc). Meloxicam (3 mg / Kg) was injected i.p. for additional post-operative analgesia and anti-inflammatory action. Mice were then returned to their cages to recover until behavioral training (~ 2 weeks).

Habituation and behavior. Mice were trained to perform a goal-directed tactile task using a custom made behavioral platform (Micallef et al., 2017). A three to four day habituation period preceded the beginning of the operant conditioning. During this period mice were handled and acclimatized to the behavioral setup. Mice were head restrained for incremental periods of time until habituated to head restraint. To maximize task engagement, a day prior to the beginning of behavioral training, mice were water restricted (1 ml/day of 10% sucrose water) and from this day onward this water regimen was maintained until the end of the experiment. Behavioral sessions lasted ~ 300 trials during which the mice typically obtained their daily water intake (1 ml per day) otherwise extra water was supplemented. Ca^{2+} imaging was performed following this habituation phase for naïve data.

Behavioral platform: Mice were head-fixed to the recording frame and their paws rested unaided on either an active (contralateral) or inactive (ipsilateral) rod coupled to a stepper motor driven by an Arduino Uno microprocessor. The stepper motor delivered a pure frequency forepaw tactile stimulus (500 ms, 200 Hz). A water port was used to deliver a water reward (10ul, 10% sucrose water) and licking frequency was recorded via a custom-made piezo-based lick sensor attached to the lick port. All behavioral tests were carried out in the dark while the animal behavior was monitored with an infrared sensitive camera (Microsoft lifecam). During the first training sessions, mice were habituated to tactile stimulus and reward delivery (typically 1-2 sessions). To establish an association between stimulus and reward, mice were able to self-initiate a trial by licking the water port which instantaneously triggered both stimulus and reward. After this habituation phase, operant conditioning was performed. **Action goal-directed task**: Background white noise (~40

DB) was played for the duration of each trial to indicate task onset and mask non-task related sounds. Tactile stimulation (200 Hz, 500 ms) was delivered after a 3-sec baseline period. Following stimulus presentation, mice were given a 1.5 sec interval to report the detection of the tactile stimulus by licking the lickport (response epoch), after which reward was made available and cued by an auditory sound (400 Hz, 200 ms). Mice were then given a 2-sec time window to retrieve the reward after which the trial terminated followed by an inter trial interval (ITI) of randomized duration (between 4 – 7 sec). Only correct responses (licks during the response epoch) were rewarded (Correct) while failure to report stimulus detection was considered an incorrect response (Incorrect). Trials with no tactile stimulation (catch trials) were randomly interleaved with stimulus trials. Licking within the response epoch during a catch trial was considered a false alarm (FA) and punished with a timeout of incremental duration (2 - 7 sec) while withhold licking was the correct response which was not rewarded, correct rejection (CR). Implementing catch trials and randomized ITI ensured that animals could not solve the task by adopting a time-based strategy. To facilitate learning, during the first training session the frequency of stimulus/catch trials was set to 90 / 10 %, respectively. The frequency of catch trials was progressively increased up to 40 % and maintained at this ratio until mice could reliably perform at expert level (≥ 80 correct response rate). On average, mice reached expert level within 4.38 ± 0.37 training sessions. **Action-suppression goal-directed task**: Background white noise (~40 DB) was played for the duration of each trial to indicate task onset and mask non-task related sounds. As in the action goal-directed task, tactile stimulation (200 Hz, 500 ms) was delivered after a 3-sec baseline period. However, following stimulus presentation, mice were trained to withhold their licking for a 1.5-sec interval. Mice were then given a 2-sec time window to retrieve the reward after which the trial terminated followed by an inter trial interval (ITI) of randomized duration (between 4 – 7 sec). Correct suppression of licking during this epoch was rewarded with sucrose water (10 µl, 10 %). Conversely, if mice licked during this interval (early lick) no reward was delivered and the trial was aborted. Catch trials were used as in the action goal-directed task. Mice learned to reliably suppress licking (≥ 80 % correct response rate) after an average 6 ± 0.85 training sessions (Figure 5 – figure supplement 2). **Switch goal-directed task.** Recordings were performed as mice transitioned from the goal-directed task to the action-suppression task. On average, mice expert in the action-task decreased performance to chance level after 2.25 ± 0.47 training sessions on the action suppression task, at which point recordings were performed.

Two photon Ca^{2+} imaging. Imaging of POm axons in forepaw S1 expressing the Ca^{2+} indicator GCaMP6f was performed in awake behaving mice through a chronic cranial window approximately 3 weeks after virus injection. Head-fixed mice were placed under a two-photon microscope (Thorlabs A-scope) and POm axons located 48 ± 6.8 μm below the pia surface were excited using a Ti:Sapphire laser (SpectraPhysics MaiTai Deepsee) tuned to λ = 940 nm and passed through a 16x water immersion objective (Nikon, 0.8 NA). GaAsP photomultiplier tubes (Hamamatsu) were used for detection. The field of view spanned 512 x 512 pixels and images were acquired at 30 Hz. To minimize photo-damage, the excitation power was adjusted online to the minimal value sufficient to record Ca^{2+} transients and the number of imaged trials for a given field of view (FOV) was restricted to a maximum of 40. During each trial, animal behavior was monitored with an infrared sensitive camera (Microsoft Lifecam). Forepaw position on the tactile stimulator was recorded using an infrared webcam and analyzed post-hoc. Due to the low resolution of the video recording, the video quality does not allow for detailed tracking of the paw, however, gross forepaw location on the tactile stimulator could be determined and any trials where the forepaw was not in contact with the stimulator were removed from further analysis.

Cannula implant and photo-inactivation of POm complex during learning and expert behavior. For optical inactivation of the POm complex, mice were injected ipsilaterally into the left POm with the inhibitory opsin AAV1.CAG.ArchT.GFP.WPRE.SV40 (60 nl; see virus injection). Following virus injection, a custom-made fiber optic cannula (FT400EMT, 400 um 0.39 NA, 2.5 mm fiber, Thorlabs) was slowly lowered down the injection track using a stereotaxic arm until the desired depth was reached (2.5 mm from pia). Dental cement (C&B metabond, Parkell Inc) was then applied around the edges of the cannula to secure it to the skull and left to dry for ~ 5 minutes. The same dental cement was used to attach a custom-made aluminum head bar (2 x 1 x 0.1 cm) to the skull for head-fixation. Meloxicam (3 mg/Kg) was injected i.p. for additional post-operative analgesia and anti-inflammatory action. Mice were then returned to their cages to recover until behavioral training (~ 3 weeks). **Behavioral procedures:** After recovery, mice were trained on the Action goal-direct task (see Habituation and Behavior). All behavioral procedures were performed using the Bpod behavioral platform (Bpod State Machine r1, Sanworks). **Photo-inactivation:** Photo-inactivation of the POm complex was achieved by delivering a light pulse

(565 nm, 5 mW) through a 400 µm optical fiber (FT400EMT, Thorlabs) directly inserted into the cannula (FT400EMT, 400 um 0.39 NA, 2.5 mm fiber, Thorlabs). A LED light source (LEDD1B, Thorlabs) coupled to a 565 nm LED filter (M565F3, Thorlabs) was used to generate the photo-stimulus. A custom-made light shield was placed over the animal's head to prevent scattered light from entering the animal visual field. Custom routines in Matlab were used to operate the behavioral platform and data acquisition. Photo-inactivation was either performed during learning, or once mice reached expert level (≥ 80% correct response rate). During expert performance, the light pulse was delivered to inactivate the POm during the stim/response epoch (2 s duration; onset 500 ms prior to stimulus onset) or during the reward epoch (2 s duration; onset at reward delivery). During a typical experimental session (~300 trials), LED-ON and LED-OFF trials were randomly interleaved at a rate of 50% each. To photo-inactivate the POm during learning of the goal-directed task, the LED was delivered during the stimulus and response epoch in all trials throughout learning (2s duration; onset 500 ms prior to stimulus onset) until mice had reached expert performance or for a maximum of 10 consecutive days of training. For control experiments, mice were stereotaxically injected into their left POm (see virus injections) with AAV1-PAM MuseeGFP (kindly provided by Daniel Scott, 60 nl) and experiments carried out as above.

Pupil tracking and analysis. To monitor engagement during the task, pupil tracking was performed in a subset of mice previously trained on the Action goal-directed task for the ArchT experiments (see above). Pupil tracking was performed when mice were expert on both the Action task and the Action-Suppression task (see Habituation and Behavior). Pupil tracking was also performed during the transition between these tasks (switching) when their correct response rate dropped to chance level (~50 %). Mice were head-fixed and the right eye illuminated with infrared light (850 nm LED, Thorlabs). This illumination did not affect pupil diameter. Behavioral sessions were performed on the same apparatus used for two photon imaging inside an aluminum soundproof optical enclosure. However, some illumination (3.48 lux) was provided as we found that the pupil became maximally dilated and a-dynamic in complete darkness**.** An IR sensitive camera (Basler aCA1300-200 um) mounting a 50 mm lens (Kowa 50mm / F2.8) was used to image pupil dynamics at 15 frames per second. Frames were triggered externally using an Arduino microprocessor connected to a Bpod (Bpod State Machine r1, Sanworks) which was then used to operate the behavioral paradigm. Changes in pupil diameter were recorded and measured online

using custom routines kindly provided by Bahr, Kremkow, Sachdev and colleagues (Bergmann, 2019).

***Ex vivo* whole cell recordings and photo-inhibition of POm neurons by ArchT activation.** Mice (P40 – P45) previously injected with ArchT in the POm (>14 days prior) were anaesthetized with isoflurane (3 – 5 % in 0.75 L/min O_2) before decapitation. The brain was then rapidly transferred and cut in an ice-cold, oxygenated solution containing (in mM): 110 choline chloride, 11.6 Na-ascorbate, 3.1 Na-pyruvate, , 26 $NaHCO_3$, 2.5 KCl, 1.25 NaH_2PO_4, 0.5 $CaCl_2$, 7 $MgCl_2$ and 10 D-Glucose (sigma). Coronal slices of the POm (300 µm thick) were cut with a vibrating microslicer (Leica Vibratome 1000S) and incubated in an incubating solution containing (in mM): 125 NaCl, 3 KCl, 1.25 NaH2PO_4, 25 $NaHCO_3$, 1 $CaCl_2$, 6 $MgCl_2$ and 10 D-Glucose at 35 ºC for 20 minutes, followed by incubation at room temperature for at least 30 minutes before recording. All solutions were continuously bubbled with 95%O_2/5%CO_2 (Carbogen). Whole-cell patch clamp somatic recordings were made from visually identified pyramidal neurons using Differential Interference Contrast (DIC) microscopy. During recording, slices were constantly perfused at ~1.5 ml/min with carbogen-bubbled artificial cerebral spinal fluid (ACSF) containing (in mM): 125 NaCl, 25 $NaHCO_3$, 3 KCl, 1.25 NaH_2PO_4, 1.2 $CaCl_2$, 0.7 $MgCl_2$ and 10 D-Glucose maintained at 30-34 ºC. Patch pipettes were pulled from borosilicate glass and had open tip resistance of 5-7 MΩ filled with an intracellular solution containing (in mM):135 potassium gluconate, 70 KCl, 10 sodium phosphocreatine, 10 HEPES, 4 Mg-ATP, 0.3 Na_2-GTP and 0.3% biocytin adjusted to pH 7.25 with KOH. Photoinhibition of POm neurons was achieved by shining a 565 nm LED light (1 s) onto the slice surface during somatic current injection steps (2s). Firing rates before and during light application were quantified and compared to the same time period of the current step injection when no light was applied (Figure 5 – figure supplement 1).

Histology. At completion of each experiment, mice were transcardially perfused with phosphate buffer (PB 0.1M) and 4% paraformaldehyde (PFA) solution. Brains were collected and post fixed overnight (~12 hrs.) in 4 % PFA at 4 ºC before being cut into 200 µm coronal slices using a vibratome (Leica VT1000 Automated Vibratome) and mounted on glass slides using mounting medium containing nuclear staining dye DAPI (Fluoroshild, Sigma). Images of the brain slices were acquired using wide-field fluorescent microscopy (Zeiss Axio Imager 2). Images were taken

such that excitation light (EYFP, 555 nm; DAPI, 430 nm) was optimized below the maximum pixel saturation value for each fluorophore. To evaluate virus (GCaMP6f, ArchT) expression profiles in the POm complex, images of brain sections were registered to the corresponding coronal plates of the Paxinos mouse brain atlas (Paxinos and Franklin, 2001). Data from out of target injections or failed viral expression were removed from further analysis.

Data analysis and statistical methods.

Ca^{2+} data. All analysis was performed using ImageJ and custom written routines in Matlab or Python. Horizontal and vertical drifts of imaging frames due to animal motion were corrected by registering each frame to a reference image based on whole-frame cross-correlation. The reference image was generated by averaging frames for a given field of view (FOV) in which motion drifts were minimal (> 15 pixels). Region of interests (ROIs) of axonal shafts or buttons were selected using the standard deviation of the entire imaging session (~ 6000 – 8000 frames) and manually drawn using the freehand tool in ImageJ. ROIs were selected so that each ROI represented a single POm axon. The activity profile was compared across all ROIs in a FOV. ROIs with similar activity profiles (where events were temporarily correlated in greater than 95 % of trials) were presumed to be axonal branches or boutons of the same neuron and replicates were excluded from analysis. On average each FOV had 19 ± 2 ROIs. Across sessions the FOVs were overlapping, however, due to the size and shear density of axonal projections, individual axons were not imaged across sessions. To calculate the baseline fluorescence (F_0) for each ROI, first the average baseline florescence intensity (across 60 frames prior to stimulus onset, 2 seconds) of each trial was taken. Second, the rolling median of these average baseline values was measured and used as F_0. Fluorescence traces are expressed as relative fluorescence changes, $\Delta F/F = (F - F_0)/F_0$. Only Ca^{2+}transients which were greater than 2x the baseline standard deviation $(F_0 + (2x\ s.d.))$ and above the threshold for a period longer than 200 ms were selected. ROIs were only considered for analysis if there was at least one Ca^{2+} transient reported during the trial (termed 'active axons'). The onset of a Ca^{2+} transient was defined as the time point at which a transient crossed the detection threshold $((F_0 + (2x\ s.d.))$. Both peak amplitude and probability of an evoked Ca^{2+} transient per trial was typically measured. According to previous studies assessing the relationship between Ca^{2+} transients and action potential firing (Wei *et al*, 2020), Ca^{2+} transient amplitude may reflect the number of action potentials whereas Ca^{2+} transient probability is independent on the number

of evoked action potentials. Average Ca^{2+} transient probability was measured as $((\frac{\Sigma\ events}{time}) / \Sigma\ trials)$. The peak amplitude (ΔF/F) was measured as the local maxima between the event onset and offset (i.e. when the falling edge of the transient crossed the threshold again). The duration (ms) of a Ca^{2+} transient was calculated as the time between the event onset and offset.

Three behaviorally relevant epochs were selected (1 second duration) for *spontaneous activity* (-2 to -1 sec, relative to stimulus onset); for *response activity* (0 to +1 sec, relative to stimulus onset) and for *reward activity* (0 to +1 sec, relative to reward delivery). In a subset of axons (n = 107 axons, 3 mice), Ca^{2+} transients were further sub-categorized as either occurring during the stimulus (0 - 500 ms) and response epochs (500 – 1000 ms) during the goal-directed task. Here, only a small portion of the axons (6 %) were active only during the stimulus, whereas most axons were active during the response (only, 38 % or combined, 56 %). Therefore, to ensure accurate analysis of Ca^{2+} transients by using an expanded temporal window, the stimulus and response epoch were merged in the reported results. For probability comparisons, all ROIs were used, while only the subset of ROIs (i.e. axons) with detectable events (greater than the threshold) were used to measure amplitude and duration. This determines the difference in number of axons used for each analysis. For direct comparison of POm activity during different epochs/behaviors, the subset of active axons with detectable Ca^{2+} events were typically used for analysis. On occasion, a mass average Ca^{2+} response was instead used, which is a mass average of all axons whether or not they had a response. Where appropriate, the variance of the peak Ca^{2+} amplitudes were compared using a F test. For displaying population activity, each row of the Ca^{2+} activity pattern is an individual axon, which is sorted by the timing of the peak amplitude for the particular behavioral condition.

Pupil tracking. Videos of pupil tracking and animal behavior were acquired and checked post hoc to remove potential artifacts due to sudden eyelid closing. Analysis of pupil dynamics were performed using a custom written algorithm in python. Briefly, pupil tracking for the entire session was split into single trials (11-sec duration) according to behavioral outcome. The average response profile was then calculated for each trial type for each mouse. Pupil dilation was monitored during a 4-sec baseline period preceding the beginning of each trial. The average peak diameter was measured as the local maxima of the average pupil response during the baseline epoch (-4 to 0 sec, relative to trial start; baseline), pre-tactile epoch (-3 to 0 sec, relative to stimulus onset, pre-tac) and post-tactile epoch (0 to +4 sec relative to stimulus onset, post-tac).

Behavior. The correct response rate was determined as d prime (the z transforms of HIT rate and FA rate d' = z(H) - z(F)) or as the fraction of correct trials over the total number of trials (HIT trials + correct rejection trials)/(stimulus trials + catch trials). The behavioral effects of POm photo-inactivation were quantified by comparing correct responses of photo-inactivation (LED-ON trials) vs. control (LED-OFF) trials, typically 150 each per experimental session. LED-ON trials and LED-OFF trials were randomly interleaved. The latency to first lick was calculated as the time of first lick occurrence after stimulus onset.

Statistical analysis. No pre-determined sample sizes were calculated prior to experiments. All statistics were performed using Prism software. The α significant level was set at 0.05. Normality of all value distributions was assessed by Shapiro-Wilk test (α = 0.05). Standard parametric tests were used only when data passed the normality test ($p > 0.05$). Non-parametric tests were used otherwise. Only two-sided tests were used. Specific statistical tests used and sample sizes are shown in figure captions or text.

Acknowledgments: We would like to thank members of the Palmer laboratory and Matthew Larkum for their helpful discussions and comments on the manuscript. We would also like to thank Verena Wimmer for her POm expertise and Ronny Bergmann, Viktor Bahr, Jens Kremkow and Robert Sachev for use of their pupil-tracking software.

Funding: This research was funded by the NHMRC (APP1086082, APP1063533, APP1085708), ARC (DP160103047) and the Sylvia and Charles Viertel Charitable Foundation.

Competing interests: Authors declare no competing interests.

Data and materials availability:

The source code for the behavioral system can be found online at https://github.com/palmerlab/behaviour_box, as well as additional documentation at https://palmerlab.github.io. Calcium imaging data is available on Dryad doi:10.5061/dryad.1rn8pk0wb.

REFERENCES:

Allen, W.E., Kauvar, I.V., Chen, M.Z., Richman, E.B., Yang, S.J., Chan, K., Gradinaru, V., Deverman, B.E., Luo, L., and Deisseroth, K. (2017). Global Representations of Goal-Directed Behavior in Distinct Cell Types of Mouse Neocortex. Neuron *94*, 891-907 e896. 10.1016/j.neuron.2017.04.017.

Alloway, K.D., Smith, J.B., Mowery, T.M., and Watson, G.D.R. (2017). Sensory Processing in the Dorsolateral Striatum: The Contribution of Thalamostriatal Pathways. Front Syst Neurosci *11*, 53. 10.3389/fnsys.2017.00053.

Audette, N.J., Bernhard, S.M., Ray, A., Stewart, L.T., and Barth, A.L. (2019). Rapid Plasticity of Higher-Order Thalamocortical Inputs during Sensory Learning. Neuron *103*, 277-291 e274. 10.1016/j.neuron.2019.04.037.

Audette, N.J., Urban-Ciecko, J., Matsushita, M., and Barth, A.L. (2017). POm Thalamocortical Input Drives Layer-Specific Microcircuits in Somatosensory Cortex. Cereb Cortex *28*, 1312-1328. 10.1093/cercor/bhx044.

Bergmann, R., Dominiak, S., Bahr, V., Kremkow, J., Mashaat, M.A., Oraby, H., Sehara, K., Larkum, M.E., Sachdev, R.N. (2019). Coordination of behavior in an Air Track maze: Sequential movement of whiskers, the maze and eyes.

Bradley, M.M., Miccoli, L., Escrig, M.A., and Lang, P.J. (2008). The pupil as a measure of emotional arousal and autonomic activation. Psychophysiology *45*, 602-607. 10.1111/j.1469-8986.2008.00654.x.

Bruno, R.M., and Sakmann, B. (2006). Cortex is driven by weak but synchronously active thalamocortical synapses. Science *312*, 1622-1627. 10.1126/science.1124593.

Casagrande, V.A., Sary, G., Royal, D., and Ruiz, O. (2005). On the impact of attention and motor planning on the lateral geniculate nucleus. Prog Brain Res *149*, 11-29. 10.1016/S0079-6123(05)49002-0.

Castejon, C., Barros-Zulaica, N., and Nunez, A. (2016). Control of Somatosensory Cortical Processing by Thalamic Posterior Medial Nucleus: A New Role of Thalamus in Cortical Function. PLoS One *11*, e0148169. 10.1371/journal.pone.0148169.

Clasca, F., Rubio-Garrido, P., and Jabaudon, D. (2012). Unveiling the diversity of thalamocortical neuron subtypes. Eur J Neurosci *35*, 1524-1532. 10.1111/j.1460-9568.2012.08033.x.

Deschenes, M., Veinante, P., and Zhang, Z.W. (1998). The organization of corticothalamic projections: reciprocity versus parity. Brain Res Brain Res Rev *28*, 286-308.

El-Boustani, S., Sermet, B.S., Foustoukos, G., Oram, T.B., Yizhar, O., and Petersen, C.C.H. (2020). Anatomically and functionally distinct thalamocortical inputs to primary and secondary mouse whisker somatosensory cortices. Nat Commun *11*, 3342. 10.1038/s41467-020-17087-7.

Gambino, F., Pages, S., Kehayas, V., Baptista, D., Tatti, R., Carleton, A., and Holtmaat, A. (2014). Sensory-evoked LTP driven by dendritic plateau potentials in vivo. Nature *515*, 116-119. 10.1038/nature13664.

765 Groh, A., Bokor, H., Mease, R.A., Plattner, V.M., Hangya, B., Stroh, A., Deschenes, M., and
766 Acsady, L. (2014). Convergence of cortical and sensory driver inputs on single
767 thalamocortical cells. Cereb Cortex *24*, 3167-3179. 10.1093/cercor/bht173.
768 Guo, Z.V., Inagaki, H.K., Daie, K., Druckmann, S., Gerfen, C.R., and Svoboda, K. (2017).
769 Maintenance of persistent activity in a frontal thalamocortical loop. Nature *545*, 181-186.
770 10.1038/nature22324.
771 Hong, Y.K., Lacefield, C.O., Rodgers, C.C., and Bruno, R.M. (2018). Sensation, movement and
772 learning in the absence of barrel cortex. Nature *561*, 542-546. 10.1038/s41586-018-0527-y.
773 Jahanshahi, M., Obeso, I., Rothwell, J.C., and Obeso, J.A. (2015). A fronto-striato-subthalamic-
774 pallidal network for goal-directed and habitual inhibition. Nat Rev Neurosci *16*, 719-732.
775 10.1038/nrn4038.
776 Jones, E.G. (2007). The Thalamus. .
777 Kamishina, H., Conte, W.L., Patel, S.S., Tai, R.J., Corwin, J.V., and Reep, R.L. (2009). Cortical
778 connections of the rat lateral posterior thalamic nucleus. Brain Res *1264*, 39-56.
779 10.1016/j.brainres.2009.01.024.
780 Kepecs, A., Uchida, N., Zariwala, H.A., and Mainen, Z.F. (2008). Neural correlates, computation
781 and behavioural impact of decision confidence. Nature *455*, 227-231. 10.1038/nature07200.
782 Kobak, D., Brendel, W., Constantinidis, C., Feierstein, C.E., Kepecs, A., Mainen, Z.F., Qi, X.L.,
783 Romo, R., Uchida, N., and Machens, C.K. (2016). Demixed principal component analysis of
784 neural population data. Elife *5*. 10.7554/eLife.10989.
785 Komura, Y., Tamura, R., Uwano, T., Nishijo, H., Kaga, K., and Ono, T. (2001). Retrospective and
786 prospective coding for predicted reward in the sensory thalamus. Nature *412*, 546-549.
787 10.1038/35087595.
788 Lacefield, C.O., Pnevmatikakis, E.A., Paninski, L., and Bruno, R.M. (2019). Reinforcement
789 Learning Recruits Somata and Apical Dendrites across Layers of Primary Sensory Cortex.
790 Cell Rep *26*, 2000-2008 e2002. 10.1016/j.celrep.2019.01.093.
791 Li, N., Chen, T.W., Guo, Z.V., Gerfen, C.R., and Svoboda, K. (2015). A motor cortex circuit for
792 motor planning and movement. Nature *519*, 51-56. 10.1038/nature14178.
793 Mease, R.A., Metz, M., and Groh, A. (2016). Cortical Sensory Responses Are Enhanced by the
794 Higher-Order Thalamus. Cell Rep *14*, 208-215. 10.1016/j.celrep.2015.12.026.
795 Meyer, H.S., Wimmer, V.C., Hemberger, M., Bruno, R.M., de Kock, C.P., Frick, A., Sakmann,
796 B., and Helmstaedter, M. (2010). Cell type-specific thalamic innervation in a column of rat
797 vibrissal cortex. Cereb Cortex *20*, 2287-2303. 10.1093/cercor/bhq069.
798 Micallef, A.H., Takahashi, N., Larkum, M.E., and Palmer, L.M. (2017). A Reward-Based
799 Behavioral Platform to Measure Neural Activity during Head-Fixed Behavior. Front Cell
800 Neurosci *11*, 156. 10.3389/fncel.2017.00156.
801 Moore, J.D., Mercer Lindsay, N., Deschenes, M., and Kleinfeld, D. (2015). Vibrissa Self-Motion
802 and Touch Are Reliably Encoded along the Same Somatosensory Pathway from Brainstem
803 through Thalamus. PLoS Biol *13*, e1002253. 10.1371/journal.pbio.1002253.

Morgenstern, N.A., Bourg, J., and Petreanu, L. (2016). Multilaminar networks of cortical neurons integrate common inputs from sensory thalamus. Nat Neurosci *19*, 1034-1040. 10.1038/nn.4339.

Oh, S.W., Harris, J.A., Ng, L., Winslow, B., Cain, N., Mihalas, S., Wang, Q., Lau, C., Kuan, L., Henry, A.M., et al. (2014). A mesoscale connectome of the mouse brain. Nature *508*, 207-214. 10.1038/nature13186.

Paxinos, G., and Franklin, K.J. (2001). The Mouse Brain in Stereotaxic Coordinates.

Poort, J., Khan, A.G., Pachitariu, M., Nemri, A., Orsolic, I., Krupic, J., Bauza, M., Sahani, M., Keller, G.B., Mrsic-Flogel, T.D., and Hofer, S.B. (2015). Learning Enhances Sensory and Multiple Non-sensory Representations in Primary Visual Cortex. Neuron *86*, 1478-1490. 10.1016/j.neuron.2015.05.037.

Poulet, J.F., Fernandez, L.M., Crochet, S., and Petersen, C.C. (2012). Thalamic control of cortical states. Nat Neurosci *15*, 370-372. 10.1038/nn.3035.

Poulet, J.F., and Petersen, C.C. (2008). Internal brain state regulates membrane potential synchrony in barrel cortex of behaving mice. Nature *454*, 881-885. 10.1038/nature07150.

Ramcharan, E.J., Gnadt, J.W., and Sherman, S.M. (2005). Higher-order thalamic relays burst more than first-order relays. Proc Natl Acad Sci U S A *102*, 12236-12241. 10.1073/pnas.0502843102.

Reimer, J., Froudarakis, E., Cadwell, C.R., Yatsenko, D., Denfield, G.H., and Tolias, A.S. (2014). Pupil fluctuations track fast switching of cortical states during quiet wakefulness. Neuron *84*, 355-362. 10.1016/j.neuron.2014.09.033.

Saalmann, Y.B., and Kastner, S. (2011). Cognitive and perceptual functions of the visual thalamus. Neuron *71*, 209-223. 10.1016/j.neuron.2011.06.027.

Schmitt, L.I., Wimmer, R.D., Nakajima, M., Happ, M., Mofakham, S., and Halassa, M.M. (2017). Thalamic amplification of cortical connectivity sustains attentional control. Nature *545*, 219-223. 10.1038/nature22073.

Sherman, S.M., and Guillery, R.W. (1996). Functional organization of thalamocortical relays. J Neurophysiol *76*, 1367-1395. 10.1152/jn.1996.76.3.1367.

Stringer, C., Pachitariu, M., Steinmetz, N., Reddy, C.B., Carandini, M., and Harris, K.D. (2019). Spontaneous behaviors drive multidimensional, brainwide activity. Science *364*, 255. 10.1126/science.aav7893.

Takahashi, N., Moberg, S., Zolnik, T.A., Catanese, J., Sachdev, R.N.S., Larkum, M.E., and Jaeger, D. (2021). Thalamic input to motor cortex facilitates goal-directed action initiation. Curr Biol *31*, 4148-4155 e4144. 10.1016/j.cub.2021.06.089.

Takahashi, N., Oertner, T.G., Hegemann, P., and Larkum, M.E. (2016). Active cortical dendrites modulate perception. Science *354*, 1587-1590. 10.1126/science.aah6066.

Trageser, J.C., and Keller, A. (2004). Reducing the uncertainty: gating of peripheral inputs by zona incerta. J Neurosci *24*, 8911-8915. 10.1523/JNEUROSCI.3218-04.2004.

Tye, K.M., and Uchida, N. (2018). Editorial overview: Neurobiology of behavior. Curr Opin Neurobiol *49*, iv-ix. 10.1016/j.conb.2018.02.019.

Urbain, N., Salin, P.A., Libourel, P.A., Comte, J.C., Gentet, L.J., and Petersen, C.C.H. (2015). Whisking-Related Changes in Neuronal Firing and Membrane Potential Dynamics in the Somatosensory Thalamus of Awake Mice. Cell Rep *13*, 647-656. 10.1016/j.celrep.2015.09.029.

van Groen, T., and Wyss, J.M. (1992). Projections from the laterodorsal nucleus of the thalamus to the limbic and visual cortices in the rat. J Comp Neurol *324*, 427-448. 10.1002/cne.903240310.

Wilke, M., Mueller, K.M., and Leopold, D.A. (2009). Neural activity in the visual thalamus reflects perceptual suppression. Proc Natl Acad Sci U S A *106*, 9465-9470. 10.1073/pnas.0900714106.

Williams, L.E., and Holtmaat, A. (2019). Higher-Order Thalamocortical Inputs Gate Synaptic Long-Term Potentiation via Disinhibition. Neuron *101*, 91-102 e104. 10.1016/j.neuron.2018.10.049.

Wimmer, R.D., Schmitt, L.I., Davidson, T.J., Nakajima, M., Deisseroth, K., and Halassa, M.M. (2015). Thalamic control of sensory selection in divided attention. Nature *526*, 705-709. 10.1038/nature15398.

Xu, N.L., Harnett, M.T., Williams, S.R., Huber, D., O'Connor, D.H., Svoboda, K., and Magee, J.C. (2012). Nonlinear dendritic integration of sensory and motor input during an active sensing task. Nature *492*, 247-251. 10.1038/nature11601.

Yamashita, T., Vavladeli, A., Pala, A., Galan, K., Crochet, S., Petersen, S.S.A., and Petersen, C.C.H. (2018). Diverse Long-Range Axonal Projections of Excitatory Layer 2/3 Neurons in Mouse Barrel Cortex. Front Neuroanat *12*, 33. 10.3389/fnana.2018.00033.

Yamawaki, N., and Shepherd, G.M. (2015). Synaptic circuit organization of motor corticothalamic neurons. J Neurosci *35*, 2293-2307. 10.1523/JNEUROSCI.4023-14.2015.

Yu, J., Gutnisky, D.A., Hires, S.A., and Svoboda, K. (2016). Layer 4 fast-spiking interneurons filter thalamocortical signals during active somatosensation. Nat Neurosci *19*, 1647-1657. 10.1038/nn.4412.

Zhang, W., and Bruno, R.M. (2019). High-order thalamic inputs to primary somatosensory cortex are stronger and longer lasting than cortical inputs. Elife *8*. 10.7554/eLife.44158.

Zhou, H., Schafer, R.J., and Desimone, R. (2016). Pulvinar-Cortex Interactions in Vision and Attention. Neuron *89*, 209-220. 10.1016/j.neuron.2015.11.034.

FIGURE CAPTIONS:

Figure 1 | Ca^{2+} activity of POm axonal projections in forepaw S1 during tactile goal-directed behavior.

(A) The Ca^{2+} indicator GCaMP6f was locally injected into the POm (bottom) which sends axonal projections to layer 1 and layer 5 of the forepaw S1 (top). Inset, In vivo two-photon Ca^{2+} image of POm axonal projections in forepaw S1 (depth, 60 μm; scalebar, 10 μm). **(B)** Two-photon Ca^{2+} imaging of GCaMP6f-expressing POm axons in forepaw S1 was performed in head-restrained mice trained to report the detection of a tactile stimulus (200 Hz, 500 ms) by licking a reward port. Correct responses (HIT) were rewarded with sucrose water reward (10μl, 10% sucrose). **(C)** Top, Raster plot showing a typical behavioral response (licks) sorted into correct HIT performance and Catch (no-stimulus) trials. Grey, spontaneous; red, tactile stimulus; green, response epoch; blue, reward epoch. Blue line, reward delivery. Bottom, example of Ca^{2+} activity pattern during correct performance and Catch trials from the POm axon in (A). Each row represents a single trial, sorted according to trial number. **(D)** Mass average with SEM (shaded area) of all stimulus-evoked Ca^{2+} transients in all axons during correct goal-directed performance (HIT; black). Behavioral epochs indicated by color bars (red, stimulus; green, response; blue, reward) **(E)** Probability of evoking a Ca^{2+} response during correct HIT behavior (black) compared with tactile-evoked activity in the naïve state (grey, n = 113 axons; Mann-Whitney test). **(F)** Top, Ca^{2+} activity pattern during HIT performance in the tactile goal-directed task. Each row is an independent axon normalized to maximum fluorescence and sorted by the timing of the peak amplitude (grey, baseline; red, stimulus; green, response epoch; blue, reward epoch). Red lines, stimulus delivery. Dashed line, reward delivery. Bottom, Average Ca^{2+} response in POm axons active during the stimulus and response epoch (green), reward epoch (blue); baseline (no behavior; grey). **(G)** The probability of a Ca^{2+} transient in POm axons during baseline (grey), response epoch (green), reward epoch (blue). n = 418 axons, 11 mice. Friedman test + Dunn's multiple comparisons test. **(H)** The amplitude of Ca^{2+} transients in POm axons evoked during baseline (grey), response epoch (green), reward epoch (blue). n = 239 axons, 11 mice with evoked Ca^{2+} transients. Friedman test + Dunn's multiple comparisons test. **(I)** Top, Average lick frequency during spontaneous (grey), stim/response (green) and reward (blue) epochs during correct HIT behavior. Bottom, Histogram of Ca^{2+} transient probability in POm axons. * $P < 0.05$, *** $P < 0.001$, **** $P < 0.0001$.

Figure 2 | POm axonal projections in forepaw S1 have greatest activity during correct behavioral performance in a tactile goal-directed task.

(A) Behavioral task design. Two-photon Ca^{2+} imaging of GCaMP6f-expressing POm axons in forepaw S1 was performed in head-restrained mice trained to report the detection of a tactile stimulus (200 Hz, 500 ms) by licking a reward port. Mice received sucrose water reward (10µl, 10% sucrose) during correct responses (HIT), whereas incorrect responses (MISS) were unrewarded. **(B)** Ca^{2+} activity patterns in POm axons with Ca^{2+} transients evoked during HIT (top) and MISS (bottom) behavior during the tactile goal-directed task (n = 159 axons, 6 mice). Grey, baseline; Red, stimulus; Green, response epoch; Blue, reward epoch. Each row is an independent axon normalized to maximum fluorescence and sorted by the timing of the peak amplitude for both HIT and MISS trials. Orange bar denotes axons that were 'active' during the behavior. **(C)** The probability of a Ca^{2+} transient evoked during the response epoch in HIT (solid), MISS (empty) and false alarm (FA; dark grey) behavior. Wilcoxon matched-pairs signed rank test (HIT vs MISS) and Mann-Whitney test (FA vs HIT and MISS). **(D)** The probability of a Ca^{2+} transient evoked during the same time period as the reward epoch in HIT (solid), MISS (empty) and baseline (light grey). Friedman test + Dunn's multiple comparisons test. * $P < 0.05$, *** $P < 0.001$, **** $P < 0.0001$.

Figure 3 | Ca^{2+} dynamics in POm axonal terminals during suppression of a goal-directed action.

(A) Behavioral task design. Two-photon Ca^{2+} imaging of POm axon terminals was performed in head-restrained mice trained to suppress a previously learned goal-directed action. Mice were trained to withhold licking in response to forepaw stimulation (200 Hz, 500 ms) for 1.5 seconds to get a reward (10 µl, 10 % sucrose water). **(B)** Top, Average pupil diameter with SEM (shaded area) during correct performance in the 'suppression' goal-directed task (red) and 'action' goal-directed task (black). Bottom, Comparison of pupil dilation during the 'action' and 'suppression' goal-directed tasks in baseline, pre-tactile stimulus (pre-tac) and post-tactile stimulus (post-tac) epochs (n = 6 mice: Wilcoxon matched-pairs signed rank test). Grey line, trial start; red line, stimulus, blue line, reward delivery. **(C)** Top, Raster plot showing the typical licking response during correct performance of the task. Grey, spontaneous; Red, stimulus; Green, response epoch; Blue, reward epoch. Blue line, reward delivery. Middle, Ca^{2+} activity pattern in an example axon during HIT trials. Bottom, Average Ca^{2+} activity pattern with SEM (shaded area) in HIT trials for

the example axon (n = 17 trials). Red line, stimulus delivery; Blue line, reward delivery. **(D)** Probability of evoking a Ca^{2+} transient during HIT (correct suppression of licking behavior; red) and MISS (no suppression of licking behavior; red empty). n = 144 axons, 6 mice; Wilcoxon matched-pairs signed rank test. **(E)** Overlay of the mass average with SEM (shaded area) of the normalized Ca^{2+} activity pattern during correct performance in the Suppression goal-directed task shown in (C) (red) and Action goal-directed task (black). **(F)** Probability of evoked Ca^{2+} transients during baseline, response, and reward epochs in the 'suppression' goal-directed task (red) and 'action' goal-directed task (black). Mann-Whitney test. ** P < 0.01, *** P < 0.001, **** P < 0.0001.

Figure 4 | Ca^{2+} activity of POm axonal projections in forepaw S1 during chance performance and behavioral switching.

(A) Behavioral task design. Ca^{2+} imaging from POm axons in forepaw S1 was performed as mice transitioned from the 'action' goal-directed task to the 'action-suppression' goal-directed task (50 % correct performance, green). **(B)** Average pupil dilation during baseline, pre-tactile stimulation (pre-tac) and post-tactile stimulation (post-tac) during the 'switch' (green) and 'action' task (black; n = 6). Red bar, tactile stimulus; blue bar, reward delivery. **(C)** Example licking behavior and associated Ca^{2+} responses from an example axon during HIT (top) and MISS (bottom) trials. **(D)** (left) Individual and (right) Overlay of average with SEM (shaded area) of evoked Ca^{2+} transients during correct (green) and incorrect (light blue) performance from example in (C)). **(E)** The probability of a Ca^{2+} transient in MISS (grey) and HIT (green) trials during chance performance (grey), and expert HIT performance in 'action' (black) and 'suppression' (red) tasks. **(F)** Peak amplitude of evoked Ca^{2+} transients during HIT trials in the action (black), switch (green) and suppression (red) behavioral task. Error bars indicate the mean ± SEM. **P < 0.01, ***P < 0.001, ****P < 0.0001.

Figure 5 | Optogenetic inactivation of the POm during an active goal-directed task

(A) Left, Experimental design. The inhibitory opsin, archaerhodopsin (ArchT) was unilaterally injected into the POm and a fiber-optic cannula was chronically inserted into the brain. Right, Localized ArchT spread in POm and fiber optic track (dotted line), bar = 1 mm. POm was photo-inactivated (590 nm, 5 mW, 2 s) either 500ms prior to, and during the stimulus (S) and response

(Rs) epochs (Stim/Resp), or during the reward epoch (Rw) in expert mice performing the 'action' goal-directed task. **(B)** Behavioral performance (d prime) for LED OFF versus LED ON during the stim/response epoch (n = 9 mice). Wilcoxon matched-pairs signed rank test. **(C)** Z score during (left) HIT and (right) False Alarm for LED OFF versus LED ON during the stim/response epoch (n = 9 mice). Wilcoxon matched-pairs signed rank test. **(D)** Latency to the first response lick in LED OFF versus LED ON during the stim/response epoch. Wilcoxon matched-pairs signed rank test. **(E)** Behavioral performance (d prime) during LED OFF and LED ON during the reward epoch in expert mice performing the 'action' goal-directed task (n = 5 mice). Wilcoxon matched-pairs signed rank test. **(F)** Normalized latency to the first response lick during LED ON in the stim/response epoch (solid) and reward (empty) epoch (normalized to the latency to the first lick during LED OFF). Line, Median. Mann-Whitney test. Individual values are shown. *P < 0.05.

Figure 6| Optogenetic inactivation of the POm during learning of a goal-directed task

(A) Mice were injected with either a control AAV (GFP; green) or the inhibitory opsin, archaerhodopsin (ArchT) into the POm and trained in the 'action' goal-directed task. A fiber optic cannula was inserted to the POm and LED (590 nm, 5 mW, 2 s) was either ON (ArchT, orange; GFP, green) or OFF (ArchT, grey) during all training sessions. Dotted line indicates expert (>80 % correct) performance. **(B)** Number of training sessions required for mice to reach expert (>80 % correct) performance in mice injected with ArchT (LED OFF, grey; LED ON, orange) or GFP (LED ON, green). Kruskal-Wallis Test. **(C)** The number of sessions for mice to reach expert (>80 % correct) performance. **P < 0.01.

Figure 1 – Figure supplement 1 | Targeting and spread of AAV injections in the POm nucleus. (A) Representative example of injection site in the mouse thalamus illustrating localized viral expression in the POm nucleus. **(B)** Overlay of the virus expression profile from the injection of ChR2-EYFP (left), GCaMP6f (middle) and ArchT-GFP (right) into the POm (green). The location of the other thalamic nuclei which primarily projects to forepaw S1, the ventral posterolateral nucleus (VPL, red) is included for comparison. **(C)** Plot comparing the virus spread for the different injections.

Figure 1 – Figure supplement 2 | Mice rapidly learn the tactile goal-directed task.
(A) Behavioral task design. Mice were habituated to head-restraint and trained to report the detection of a tactile stimulus (200 Hz, 500 ms) by licking a reward port. Correct responses were rewarded with sucrose water reward (10 ul, 10 % sucrose). Incorrect responses were punished with a time-out. **(B)** Performance of mice in the tactile goal-directed task improved in subsequent sessions, taking on average 4 days to reach expert performance (> 80 % correct; n = 11 mice).

Figure 1 - Figure supplement 3 | AAV mediated expression of ChR2-eYFP in the POm nucleus of the thalamus and its axonal projections in forepaw S1.
(A) Representative example of ChR2-eYFP in the mouse thalamus illustrating localized viral expression in the POm nucleus. Left, outline of cortical slices at different rostra-caudal locations indicating the POm nucleus (green) from Paxinos and Franklin, 2001. Right, Corresponding brain sections showing the virus expression profile in the thalamus. Scale bar, 1 mm. **(B)** Top, enlarged fluorescence image showing ChR2-eYFP expression profile in POm nucleus from example in a. The location of the ventral posteromedial nucleus (VPM) and ventral posterolateral nucleus (VPL) are illustrated for comparison. Bottom, POm axonal projection profile in the forepaw area of S1 (FPS1) from example in a). Inset, Fluorescence intensity (F_{int}) measured as a function of cortical depth (in pixels (px)) in forepaw S1 (FPS1; rectangle). **(C)** Plot comparing the intensity profiles within FPS1 in 10 different animals with injections localized in the POm nucleus.

Figure 1 - Figure supplement 4 | ROI selection and exclusion criterion.
(A) Example FOV, ROIs are selected using the standard deviation (STD) image from the concatenated images of the entire imaging session. **(B)** Fluorescence traces for ROIs shown in (A).

ROI1 and $ROI_{excluded}$ have similar fluorescence activity and $ROI_{excluded}$ is excluded from further analysis. **(C)** Spearman correlation matrix of the activity profile of all ROIs from the example FOV in (A). ROIs that have a correlation greater than 95% have been removed from further analysis. Spearman correlation is performed on all FOVs to exclude correlated ROIs.

Figure 1 - Figure supplement 5 | Tactile-evoked activity of POm axons projecting to forepaw S1 in naive and expert mice.

(A) Example Ca^{2+} responses from a typical POm axon in (top) a naive mouse during forepaw tactile stimulus (200 Hz, 500 ms) and (bottom) an expert mouse during correct HIT performance in an action goal-directed task. **(B)** Peak amplitude (left) and duration (right) of evoked Ca^{2+} transients in expert (black) and naive (grey) mice. Expert data was randomised and a sample of equal size to Naive was used for statistical analysis. Mann-Whitney test was performed for significance testing.

Figure 5 - Figure supplement 1 | POm neurons are partially photo-inhibited by 590 nm LED.

(A) The inhibitory opsin, archaerhodopsin (ArchT) was unilaterally injected into the POm and after 10-14 days, the brain was sectioned into 300 μm thick slices. Whole-cell patch clamp voltage recordings were then performed in POm neurons expressing ArchT. **(B)** Voltage recording during 590 nm light exposure from an example POm neuron (top) at rest and (bottom) during a current step injection (30 pA; 2 s). **(C)** Photo-inhibition caused a decrease in evoked action potentials during different current steps (20 pA, 30 pA, 60 pA) for example in (B). Control (Ctrl) firing was determined during current step injection in the absence of LED. **(D)** Action potential firing evoked during current step injections (0 - 100 pA, 100 - 200 pA, 200 - 300 pA) was partially inhibited during LED (0 - 100 pA, $p = 0.031$; 100 - 200 pA, $p = 0.016$; 200 - 300 pA, $p = 0.004$; Wilcoxon matched-pairs signed rank test). **(E)** Voltage response at rest at the start of the LED pulse (300 ms, light orange) normalized to the steady-state 'end' voltage (300 ms prior to end of pulse; $p = 0.031$; Wilcoxon matched-pairs signed rank test). Note, photo-suppression would be less effective *in vivo* than *in vitro* due to greater light penetration and scattering.

Figure 5 - Figure supplement 2 | LED in POm does not alter goal-directed behavior.

(A) Behavioral task design. Mice were either injected with the inhibitory opsin, AAV-ArchT or

the Green Fluorescent Protein control, AAV-GFP. Mice were then habituated to head-restraint and trained to report the detection of a tactile stimulus (200 Hz, 500 ms) by licking a reward port. Correct responses were rewarded with sucrose water reward (10µl, 10% sucrose). Incorrect responses were punished with a time-out. **(B)** Number of training sessions required to reach expert performance (>80% correct) in the tactile goal-directed task in mice previously injected with AAV-ArchT (orange) or AAV-GFP (green). **(C)** Performance, measured as percent correct, in expert mice ($p = 0.15$; Unpaired t test). **(D)** Behavioral performance (d prime) for LED OFF versus ON trials (n = 9 mice) in mice previously injected with AAV-GFP (green). **(E)** Hit rate in expert mice ($p = 0.11$; Unpaired t test). **(F)** False alarm (FA) rate in expert mice ($p = 0.21$; Unpaired t test). Mice are considered expert when > 80% correct performance in the tactile goal-directed task. AAV-ArchT, orange, n = 9 mice; AAV-GFP, green, n = 9 mice. All data passed normality test (Shapiro-Wilk test).

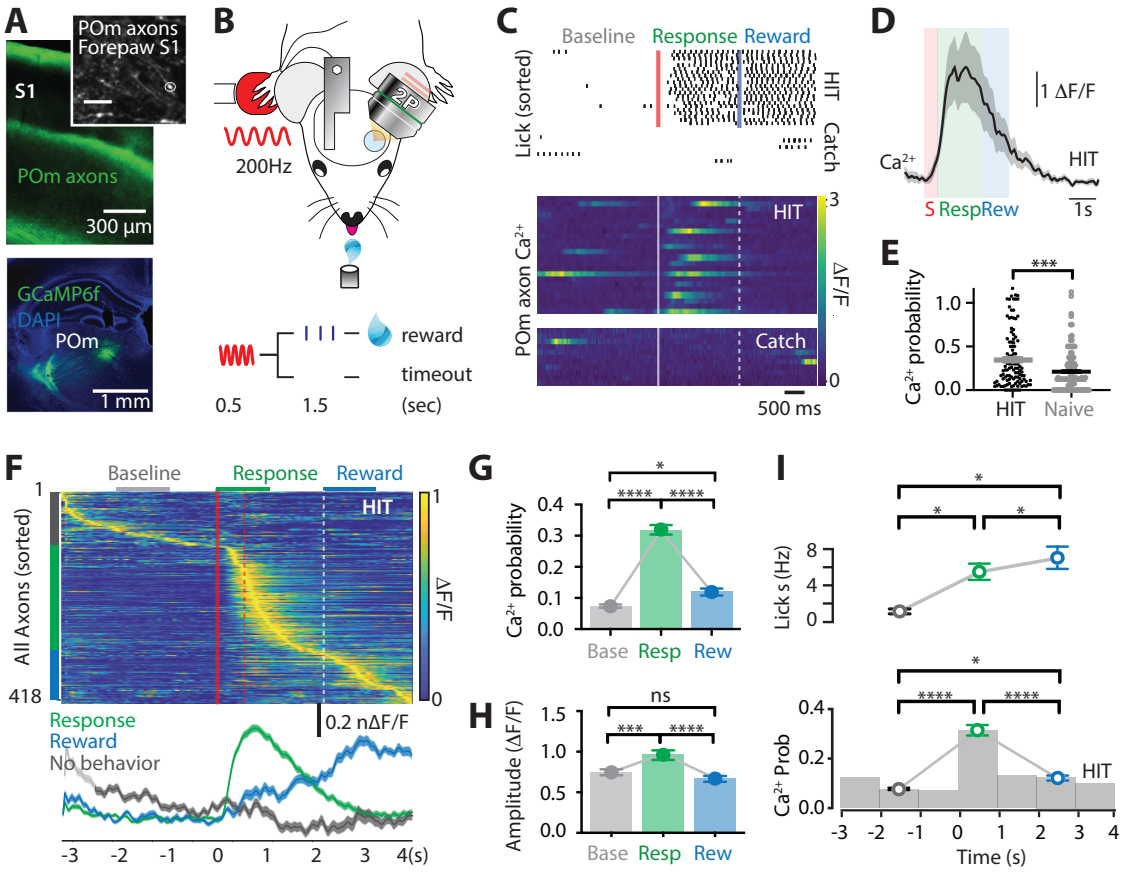
A
POm axons
Forepaw S1
S1
POm axons
300 µm
GCaMP6f
DAPI
POm
1 mm
B
2P
200Hz
reward
timeout
0.5
1.5
(sec)
C
Baseline
Response
Reward
Lick (sorted)
HIT
Catch
POm axon Ca2+
HIT
Catch
ΔF/F
3
0
500 ms
D
1 ΔF/F
Ca2+
HIT
S
Resp
Rew
1s
E
***
Ca2+ probability
1.0
0.5
0.0
HIT
Naive
F
Baseline
Response
Reward
All Axons (sorted)
1
418
HIT
ΔF/F
1
0
0.2 nΔF/F
Response
Reward
No behavior
-3
-2
-1
0
1
2
3
4(s)
G
Ca2+ probability
0.4
0.3
0.2
0.1
0.0
*
****
****
Base
Resp
Rew
H
Amplitude (ΔF/F)
1.5
1.0
0.5
0.0
ns
***
****
Base
Resp
Rew
I
Lick s (Hz)
8
4
0
*
*
*
Ca2+ Prob
0.4
0.2
0.0
*
****
****
HIT
-3
-2
-1
0
1
2
3
4
Time (s)

Figure 1

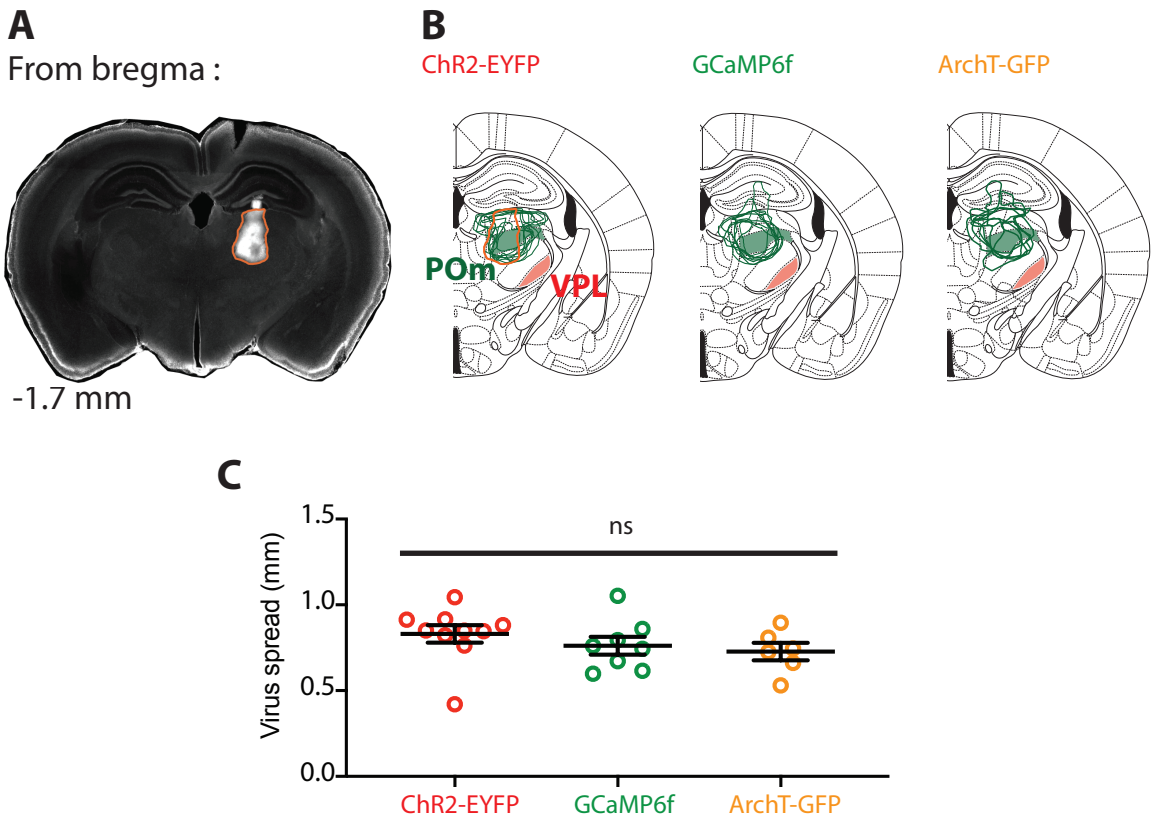

Figure 1 - Figure supplement 1

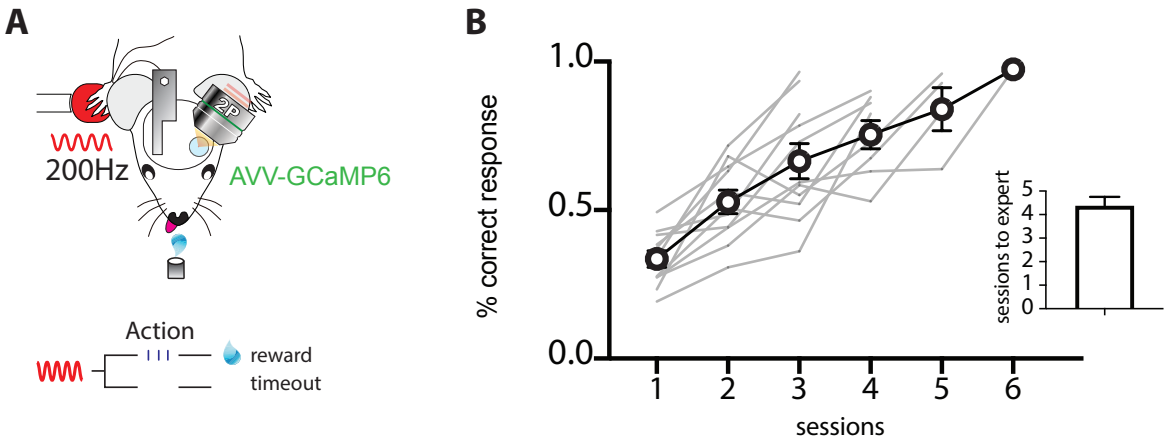

Figure 1 - Figure supplement 2

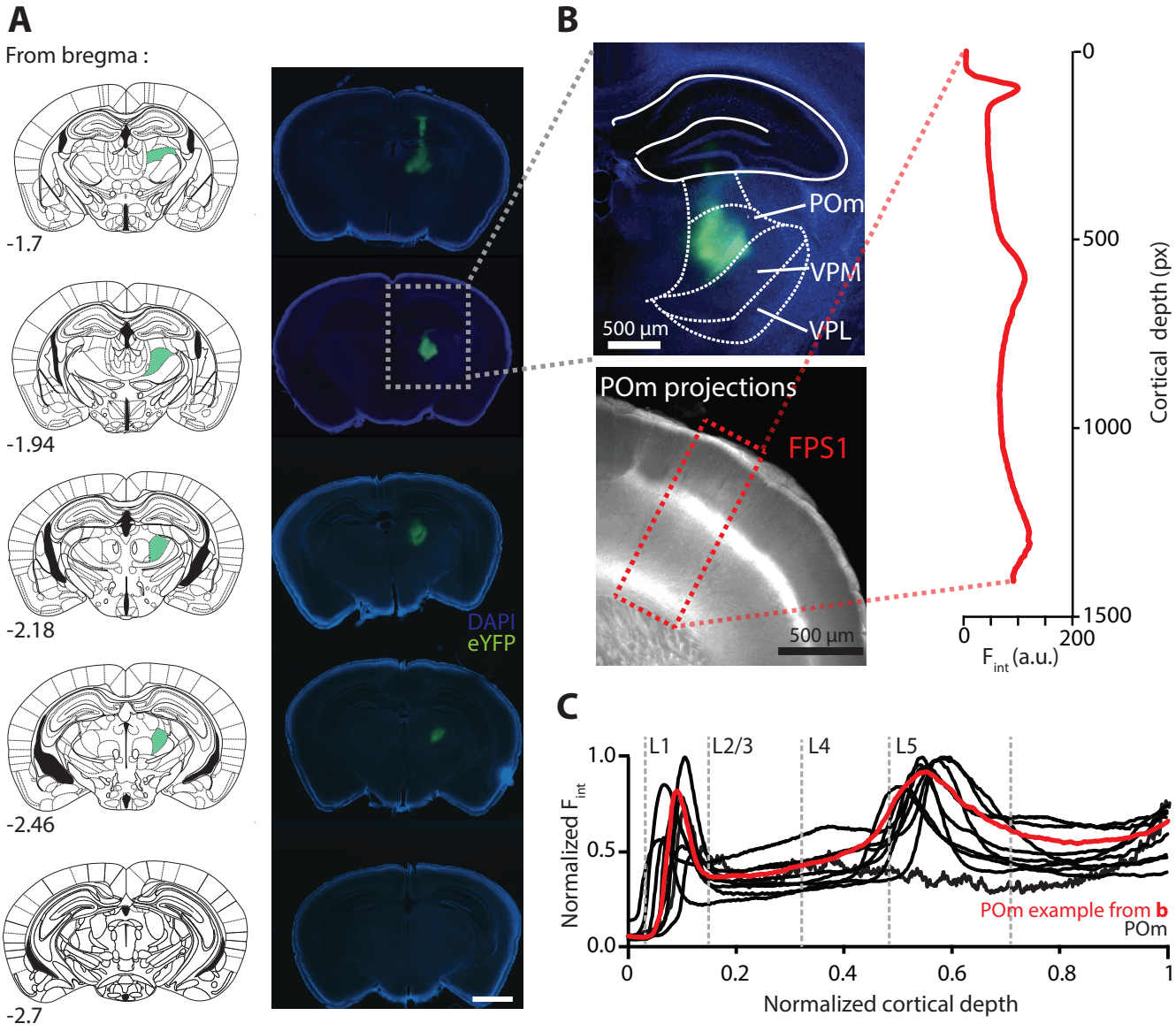

Figure 1 - Figure supplement 3

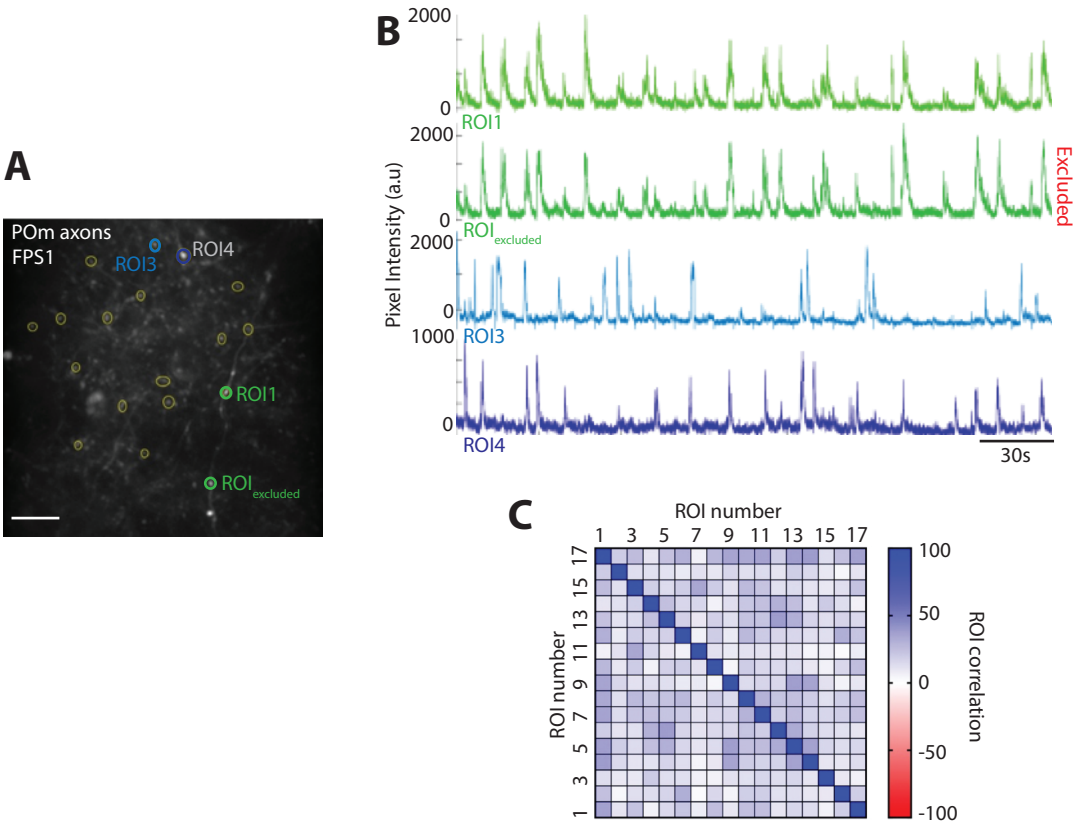

Figure 1 - Figure supplement 4

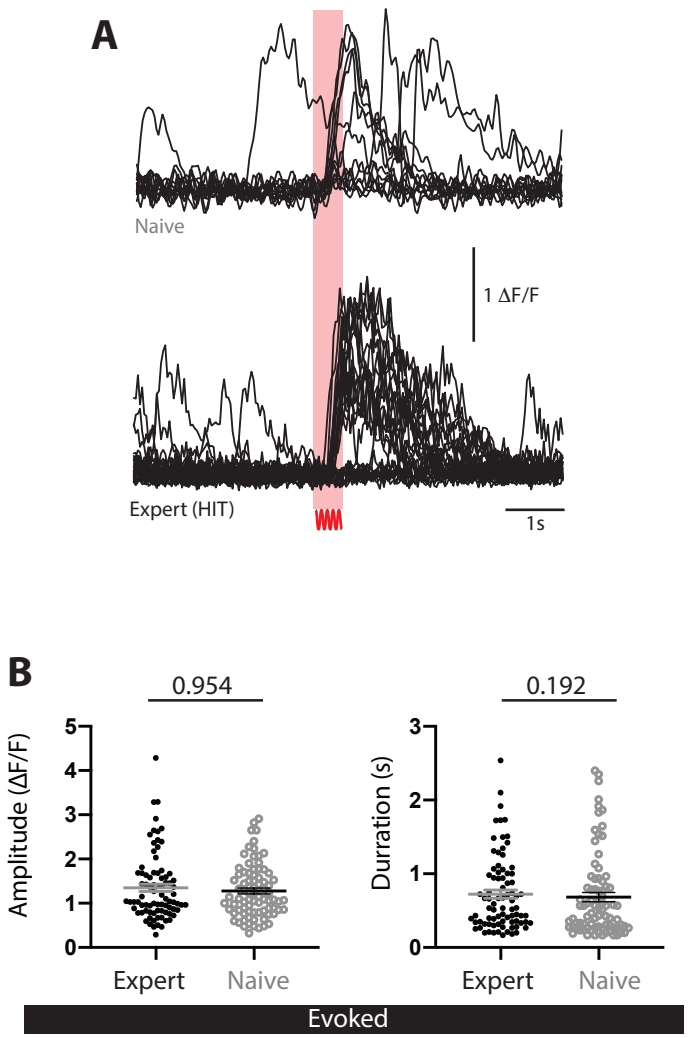

Figure 1 - Figure supplement 5

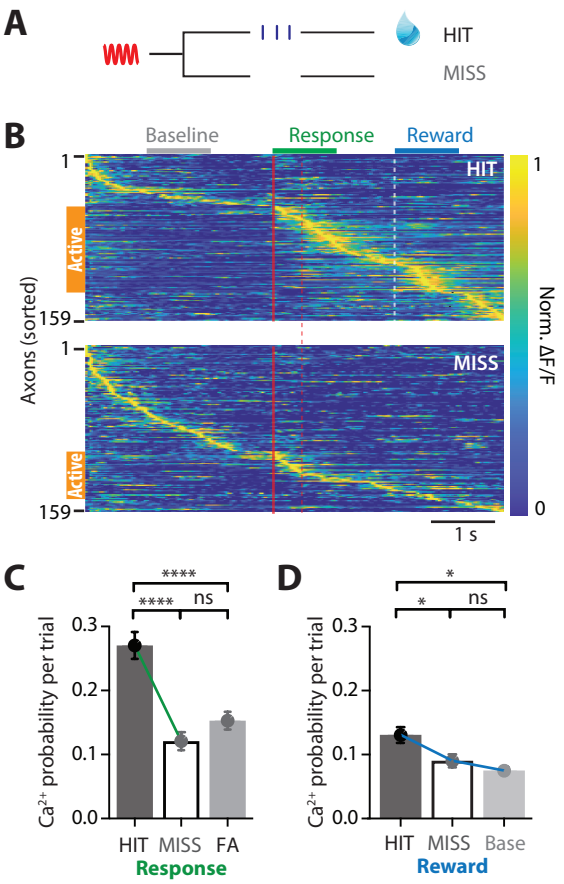
A
HIT
MISS
B
Baseline
Response
Reward
1
HIT
Active
159
Axons (sorted)
1
MISS
Active
159
1
Norm. ΔF/F
0
1 s
C
****
****
ns
Ca2+ probability per trial
0.3
0.2
0.1
0.0
HIT
MISS
FA
Response
D
*
*
ns
Ca2+ probability per trial
0.3
0.2
0.1
0.0
HIT
MISS
Base
Reward

Figure 2

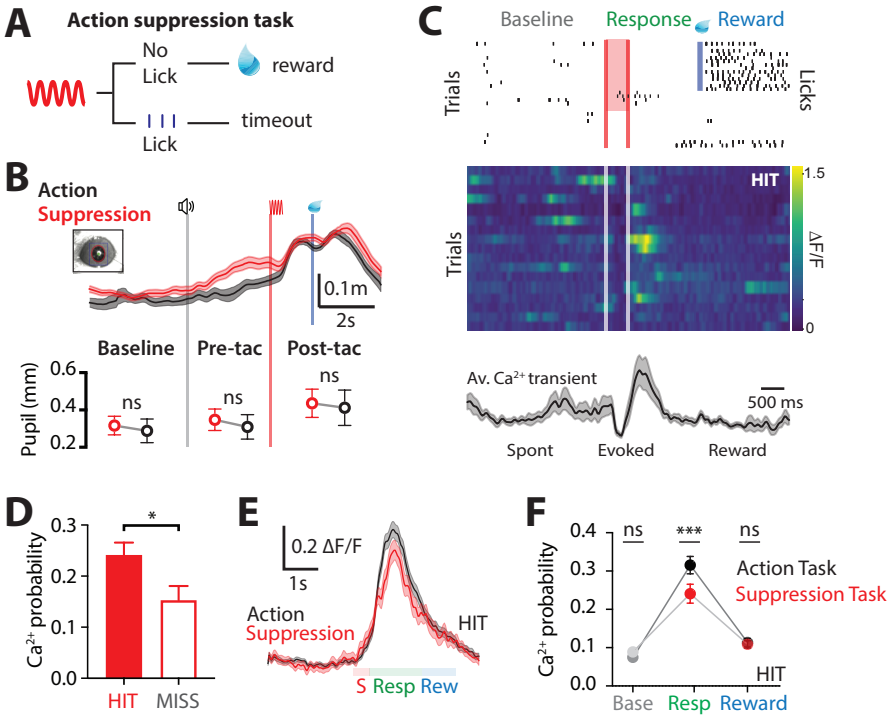
A
Action suppression task
No Lick
reward
Lick
timeout
B
Action
Suppression
0.1m
2s
Baseline
Pre-tac
Post-tac
Pupil (mm)
0.6
0.4
0.2
ns
ns
ns
C
Baseline
Response
Reward
Trials
Licks
HIT
1.5
ΔF/F
0
Av. Ca2+ transient
500 ms
Spont
Evoked
Reward
D
Ca2+ probability
0.3
0.2
0.1
0.0
*
HIT
MISS
E
0.2 ΔF/F
1s
Action
Suppression
HIT
S Resp Rew
F
Ca2+ probability
0.4
0.3
0.2
0.1
0.0
ns
***
ns
Action Task
Suppression Task
HIT
Base
Resp
Reward

Figure 3

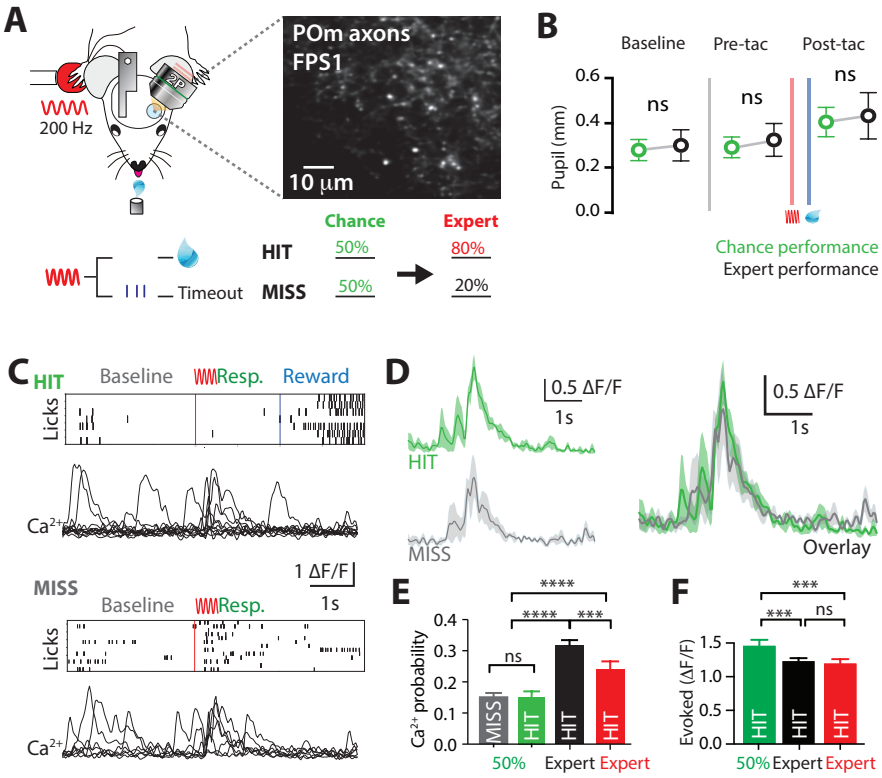
A
POm axons
FPS1
10 µm
200 Hz
Chance
Expert
HIT
50%
80%
Timeout
MISS
50%
20%
B
Baseline
Pre-tac
Post-tac
Pupil (mm)
0.6
0.4
0.2
0.0
ns
ns
ns
Chance performance
Expert performance
C
HIT
Baseline
Resp.
Reward
Licks
Ca2+
1 ΔF/F
1s
MISS
Baseline
Resp.
Licks
Ca2+
D
0.5 ΔF/F
1s
HIT
MISS
0.5 ΔF/F
1s
Overlay
E
Ca2+ probability
0.4
0.3
0.2
0.1
0.0
****
****
***
ns
MISS
HIT
HIT
HIT
50%
Expert
Expert
F
Evoked (ΔF/F)
1.5
1.0
0.5
0.0
***
***
ns
HIT
HIT
HIT
50%
Expert
Expert

Figure 4

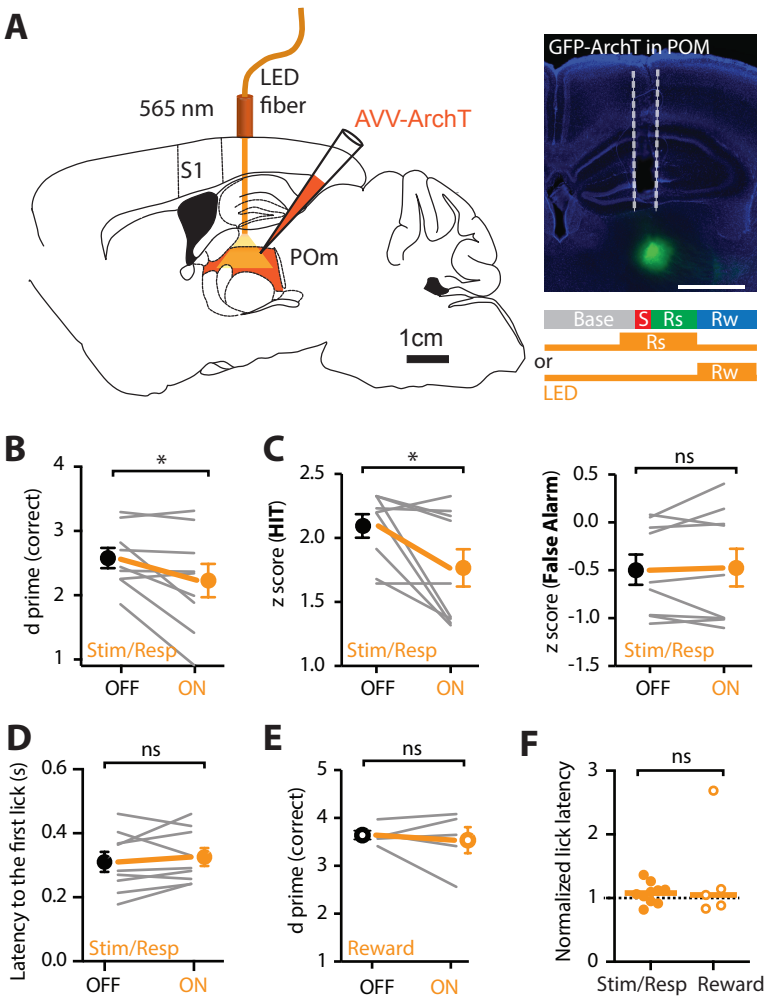
A
565 nm
LED
fiber
AVV-ArchT
S1
POm
1cm
GFP-ArchT in POM
Base
S
Rs
Rw
Rs
or
Rw
LED
B
d prime (correct)
Stim/Resp
OFF
ON
*
C
z score (HIT)
Stim/Resp
OFF
ON
*
z score (False Alarm)
Stim/Resp
OFF
ON
ns
D
Latency to the first lick (s)
Stim/Resp
OFF
ON
ns
E
d prime (correct)
Reward
OFF
ON
ns
F
Normalized lick latency
Stim/Resp
Reward
ns

Figure 5

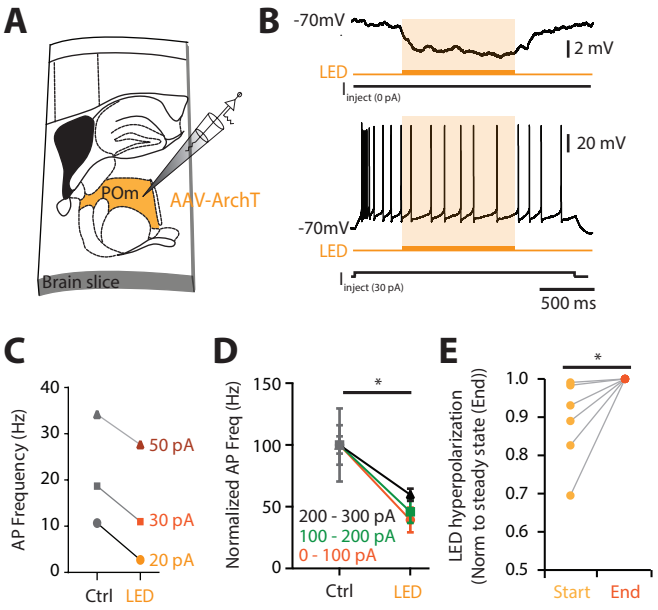

Figure 5 - Figure supplement 1

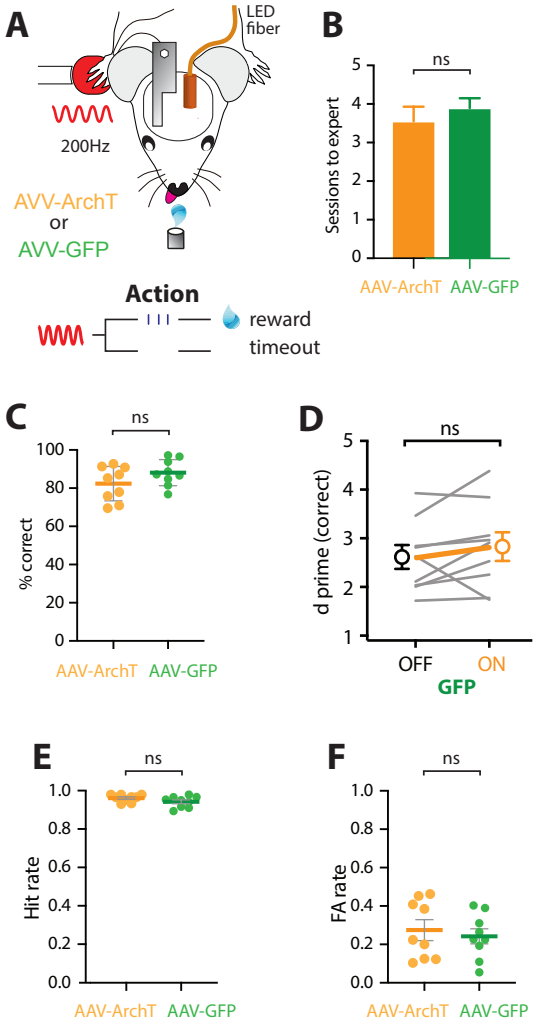

Figure 5 - Figure supplement 2

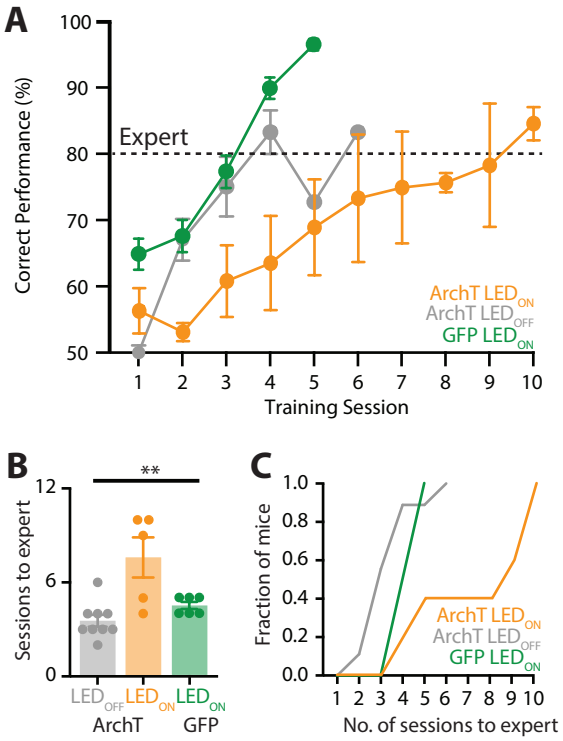
A
100
90
80
70
60
50
Correct Performance (%)
Expert
ArchT LED ON
ArchT LED OFF
GFP LED ON
1 2 3 4 5 6 7 8 9 10
Training Session
B
**
12
6
0
Sessions to expert
LED OFF
LED ON
LED ON
ArchT
GFP
C
1.0
0.8
0.6
0.4
0.2
0.0
Fraction of mice
ArchT LED ON
ArchT LED OFF
GFP LED ON
1 2 3 4 5 6 7 8 9 10
No. of sessions to expert

Figure 6